

**Dieses Dokument ist eine Zweitveröffentlichung (Manuskriptfassung)/
This is a self-archiving document (Preprint):**

Leonore Wigger, Marko Barovic, Andreas-David Brunner, Flavia Marzetta, Eyke Schöniger, Florence Mehl, Nicole Kipke, Daniela Friedland, Frederic Burdet et. al.

Multi-omics profiling of living human pancreatic islet donors reveals heterogeneous beta cell trajectories towards type 2 diabetes

Erstveröffentlichung in / First published in:

Nature metabolism. 2021, 3(7), S. 1017-1031 [Zugriff am: 30.12.2021]. Springer Nature. ISSN 2522-5812.

DOI: <https://doi.org/10.1038/s42255-021-00420-9>

Diese Version ist verfügbar / This version is available on:

<https://nbn-resolving.org/urn:nbn:de:bsz:14-qucosa2-771665>

19

20 **Multi-omics profiling of living human pancreatic islet**
21 **donors reveals heterogeneous beta cell trajectories**
22 **toward type 2 diabetes**

23

24 Leonore Wigger^{1*}, Marko Barovic^{2,3,4*}, Andreas-David Brunner^{5*}, Flavia Marzetta¹, Eyke
25 Schöniger^{2,3,4}, Florence Mehl¹, Nicole Kipke^{2,3,4}, Daniela Friedland^{2,3,4}, Frederic Burdet¹, Camille
26 Kessler¹, Mathias Lesche⁶, Bernard Thorens⁷, Ezio Bonifacio^{3,4,8}, Cristina Legido-Quigley^{9,10},
27 Pierre Barbier Saint Hilaire¹¹, Philippe Delerive¹², Andreas Dahl⁶, Christian Klose¹³, Mathias J
28 Gerl¹³, Kai Simons¹³, Daniela Aust^{14,15}, Jürgen Weitz¹⁶, Marius Distler¹⁶, Anke M Schulte¹⁷,
29 Matthias Mann^{5#}, Mark Ibberson^{1#}, Michele Solimena^{2,3,4#}

30

31 ¹Vital-IT Group, SIB Swiss Institute of Bioinformatics, Lausanne, Switzerland; ²Department of
32 Molecular Diabetology, University Hospital and Faculty of Medicine, TU Dresden; ³Paul
33 Langerhans Institute Dresden (PLID), Helmholtz Center Munich, University Hospital and Faculty
34 of Medicine, TU Dresden; ⁴German Center for Diabetes Research (DZD e.V.), Neuherberg,
35 Germany; ⁵Max Planck Institute of Biochemistry, Martinsried, Germany; ⁶DRESDEN-
36 *concept* Genome Center, c/o Center for Molecular and Cellular Bioengineering, Technische
37 Universität Dresden, Germany; ⁷Center for Integrative Genomics, University of Lausanne,
38 Lausanne Switzerland; ⁸Center for Regenerative Therapies Dresden, Faculty of Medicine and
39 Center for Molecular and Cellular Bioengineering, Technische Universität Dresden, Dresden,
40 Germany; ⁹Steno Diabetes Center Copenhagen, Gentofte, Denmark; ¹⁰King's College London,
41 London, UK; ¹¹DMPK Center, Technologie Servier, Orléans, France ¹²Institut de Recherches
42 Servier, Pôle d'Innovation Thérapeutique Métabolisme, Suresnes, France; ¹³Lipotype GmbH,
43 Dresden, Germany; ¹⁴Department of Pathology, Medical Faculty, University Hospital Carl

44 Gustav Carus, Technische Universität Dresden, Dresden, Germany; ¹⁵NCT Biobank Dresden,
45 University Hospital Carl Gustav Carus, Technische Universität Dresden, Dresden, Germany;
46 ¹⁶Department of Visceral, Thoracic and Vascular Surgery, University Hospital Carl Gustav
47 Carus, Medical Faculty, Technische Universität Dresden, Dresden, Germany; ¹⁷Sanofi-Aventis
48 Deutschland GmbH, Diabetes Research, Industriepark Höchst, 65926 Frankfurt am Main,
49 Germany.

50

51 * These authors contributed equally

52 # These authors jointly supervised this work

53

54 Corresponding authors:

55 Matthias Mann - mmann@biochem.mpg.de

56 Mark Ibberson - Mark.Ibberson@sib.swiss

57 Michele Solimena - Michele.Solimena@uniklinikum-dresden.de

58

59 Abstract

60

61 Existing studies do not sufficiently describe the molecular changes of pancreatic islet beta cells
62 leading to their deficient insulin secretion in type 2 diabetes (T2D). Here we address this
63 deficiency with a comprehensive multi-omics analysis of metabolically profiled
64 pancreatectomized living human donors stratified along the glycemic continuum from
65 normoglycemia to T2D. Islet pools isolated from surgical samples by laser-capture
66 microdissection had remarkably heterogeneous transcriptomic and proteomic profiles in
67 diabetics, but not in non-diabetic controls. Transcriptomics analysis of this unique cohort
68 revealed islet genes already differentially regulated in prediabetic individuals with impaired
69 glucose tolerance. Our findings demonstrate a progressive but disharmonic remodeling of
70 mature beta cells, challenging current hypotheses of linear trajectories toward precursor or
71 trans-differentiation stages in T2D. Further, integration of islet transcriptomics and pre-operative
72 blood plasma lipidomics data enabled us to define the relative importance of gene co-
73 expression modules and lipids positively or negatively associated with HbA1c levels, pointing to
74 potential prognostic markers.

75 Abstract

76 Most research on human pancreatic islets is conducted on samples obtained from
77 normoglycemic or diseased brain dead donors and thus cannot accurately describe the
78 molecular changes of pancreatic islet beta cells as they progress towards a state of deficient
79 insulin secretion in type 2 diabetes (T2D). Here, we conduct a comprehensive multi-omics
80 analysis of pancreatic islets obtained from metabolically profiled pancreatectomized living
81 human donors stratified along the glycemic continuum, from normoglycemia to T2D. We find
82 that islet pools isolated from surgical samples by laser-capture microdissection display
83 remarkably more heterogeneous transcriptomic and proteomic profiles in patients with diabetes
84 than in non-diabetic controls. The differential regulation of islet gene expression is already
85 observed in prediabetic individuals with impaired glucose tolerance. Our findings demonstrate a
86 progressive, but disharmonic, remodeling of mature beta cells, challenging current hypotheses
87 of linear trajectories toward precursor or trans-differentiation stages in T2D. Furthermore,
88 through integration of islet transcriptomics with pre-operative blood plasma lipidomics, we define
89 the relative importance of gene co-expression modules and lipids that are positively or
90 negatively associated with HbA1c levels, pointing to potential prognostic markers.

91

92

93

94

95

96 Introduction

97

98 Type 2 diabetes (T2D) mellitus defines a cluster of genetically complex pathological states
99 characterized by persistent hyperglycemia, often leading to cardiovascular complications,
100 kidney failure, retinopathy and neuropathies. Affecting more than 450 million people, with rising
101 incidence rates over the past decades, this syndrome is a major threat for public health and
102 society globally¹. Common determinant and ultimate cause of T2D is the inability of pancreatic
103 islet beta cells to secrete insulin in adequate amounts relative to insulin sensitivity, in the
104 absence of evidence for their autoimmune destruction or a monogenetic deficit. Beta cell failure
105 typically results from a lengthy process spanning many years. Remarkably, however, it can be
106 rapidly reverted upon bariatric surgery or severe caloric restriction^{2,3}. These observations argue
107 against the occurrence of major beta cell apoptosis in T2D, especially since adult beta cells
108 hardly replicate, while robust evidence of beta cell neogenesis after puberty is also lacking.
109 Hence, the prevailing opinion is that persistent metabolic stress drives mature beta cells to
110 phenotypically de-differentiate into progenitor cells or trans-differentiate into other islet
111 endocrine cell types over time⁴⁻⁶. As the pathogenesis of beta cell dysfunction in T2D remains
112 largely unclear, the diagnosis of this disease relies on accepted, surrogate parameters and
113 cutoffs that have been primarily developed for clinical practice to optimize therapeutic
114 interventions⁷.

115

116 Insight into molecular alterations associated with impaired insulin secretion in T2D has been
117 largely obtained from pancreatic islets isolated enzymatically from brain-dead or cadaveric
118 subjects classified according to a categorical division into non-diabetic and diabetic, rather than
119 on a continuum from euglycemia to steady hyperglycemia. This approach has multiple

120 shortcomings⁸. Briefly, islet researchers do not generally have access to extensive clinical and
121 laboratory information about the donors prior to their admission to an intensive therapy unit⁹.
122 Moreover, the islet state is perturbed by the metabolic stress associated with a terminal
123 condition and the related pharmacological treatments^{10,11}. Enzymatic isolation of islets and their
124 *in vitro* culture can further change their molecular profile^{12,13}. In the attempt to overcome, at least
125 in part, these limitations, we established a complementary platform for the procurement of islets
126 which relies on the collection and analysis of pancreatic specimens from metabolically profiled
127 living donors undergoing pancreatectomy for a variety of disorders^{8,14}. We showed that this
128 approach is very reproducible and scalable and provides a novel view on transcriptomic and
129 functional alterations in pancreatic islets of subjects with T2D¹⁵⁻¹⁷

130

131 The aim of the present study has been to profile in greater detail gene expression changes
132 occurring along the progression from euglycemia to long-standing T2D in human islets *in situ*
133 and to integrate this knowledge with clinical traits, circulating lipid levels and the islet proteome,
134 hence enabling inferences about the mechanisms driving islet dysfunction and the identification
135 of potential biomarkers for it.

136 Results

137 Living donors enable islet studies along progression to T2D

138

139 To gain insight into the history of islet cell deterioration along the progression from normal
140 glycemic regulation to T2D, we collected surgical pancreatic tissue samples from 133
141 metabolically phenotyped pancreatectomized patients (PPP). Eighteen were non-diabetic (ND),
142 41 had impaired glucose tolerance (IGT), 35 Type 3c Diabetes (T3cD) and 39 T2D (Fig. 1A and
143 Fig. 1B). These group assignments were based on glycemic values at fasting and at the 2 h
144 time point of an oral glucose tolerance test (OGTT) using the thresholds defined in the

145 guidelines of the American Diabetes Association⁷, or, when applicable, on a previously
146 established diagnosis of T2D. In this cohort, 51.9% were males and the mean age was
147 65.36 ± 11.54 years, with ND PPP being on average younger than the other three groups (Fig.
148 1C and Supplementary Table 1). The body mass index (BMI) was significantly lower in ND
149 compared to IGT, T3cD and T2D PPP. The HbA1c value, as a parameter of longer-term
150 glycemia, was 5.25 ± 0.3 in ND, 5.75 ± 0.42 in IGT, 6.29 ± 0.95 in T3cD and 7.41 ± 1.29 in T2D
151 PPP (Fig. 1C and Supplementary Table 1). Moreover, based on histopathology, malignant
152 tumors occurred in 50%, 60.97%, 74.29% and 69.23% of ND, IGT, T3cD, and T2D PPP,
153 respectively (Supplementary Table 1).

154

155 Islet gene expression drifts with glycemetic deterioration

156

157 Gene expression profiles of islets isolated by laser capture microdissection (LCM) from resected
158 and snap-frozen pancreas samples of ND, IGT, T3cD and T2D PPP were assessed by RNA
159 sequencing. After removal of genes with low expression levels, the overall islet transcriptome
160 encompassed 19,119 genes, of which $14,699 \pm 693$ were present (raw read counts >0) in ND
161 PPP, $14,967 \pm 455$ in IGT PPP, $14,939 \pm 493$ in T3cD PPP and $14,997 \pm 428$ in T2D PPP. Genes
162 with a fold change (FC) > 1.5 and a false discovery rate (FDR) ≤ 0.05 were considered to be
163 differentially expressed (DE) between the groups. Multiple group comparison by linear modeling
164 was performed (Supplementary Table 2). Subsequent pairwise group comparisons of IGT vs.
165 ND, T3cD vs. ND and T2D vs. ND revealed an exacerbation of gene dysregulation with
166 deterioration of glycemetic control (Fig. 2A). Notably, no DE islet genes were identified between
167 IGT vs. ND PPP, while 161 and 650 DE genes were found between T3cD vs. ND PPP and T2D
168 vs. ND PPP, respectively (Fig. 2A and Supplementary Table 2).

169

170 Restricting the transcriptomic analysis to libraries in which insulin (*INS*) was the most expressed
171 gene resulted in the retention of islet datasets from 15 ND, 35 IGT, 21 T3cD and 24 T2D
172 subjects, without substantially affecting the overall composition of the cohort in regard to
173 diabetes status and major descriptive parameters (Supplementary Table 3). Deconvolution
174 analysis indicated that in 78.3% of retained samples the proportion of beta cells was >50%
175 (Extended data Fig. S1), supporting the choice of this strategy to discriminate samples
176 especially enriched in beta cell transcripts. This analysis further pointed to the overall
177 enrichment in beta cell content of the LCM isolated islets in comparison to another large study
178 based on islets isolated by enzymatic digestion (median beta cell:non-beta endocrine cell ratio
179 3.98:1 and 1.4:1)¹⁸. This enrichment can conceivably be attributed to the selectivity of the LCM
180 isolation procedure for beta cell rich areas due to their higher autofluorescence. Despite the
181 expected reduction in statistical power due to ~ 30% smaller size of this "restricted" cohort (92
182 samples retained from 133), the number of significantly DE genes increased in the multiple
183 group comparison, as well as in pairwise comparisons between islets of T2D vs. ND PPP by
184 51% to 984 (782 up, 202 down), and by 59% to 256 (209 up, 47 down) between islets of T3cD
185 vs. ND PPP (Fig. 2A, Supplementary Table 4). Seven of the 984 DE genes are among the
186 putative effectors of GWAS risk loci for T2D (<https://t2d.hugeamp.org/>), two upregulated
187 (*SGSM2* and *BCL2*) and five downregulated (*RASGRP1*, *G6PC2*, *SLC2A2*, *ZMAT4* and
188 *PLUT*)¹⁹, while most of the remaining genes have not been previously reported to be altered in
189 islets of subjects with T2D^{14,20}.

190

191 Among the DE genes in islets of T2D PPP, *INF2* and *AKR7L* were negatively correlated in a
192 moderate fashion with duration of the disease measured in years (Spearman correlation
193 coefficient -0.32 and -0.41 respectively), albeit they were both upregulated relative to islets of
194 ND PPP. Most notably, this filtering step enabled, for the first time, the identification of 185 DE
195 genes between islets of IGT vs. ND PPP. Most of these DE genes were upregulated (181/185),

196 and 98 also differentially regulated with the same directionality (97 up, 1 down) between islets of
197 T2D vs. ND PPP. Intriguingly, and apparently at variance with previous findings²¹, the proposed
198 T2D risk genes *ARAP1* and its neighboring gene *STARD10* were both upregulated and among
199 the 77 genes differentially regulated in islets of IGT PPP only. No islet cell type specific genes²²
200 were enriched in any of the differential expression analyses. Furthermore, no shift of islet cell
201 type proportions with the progression of the disease was observed in the deconvolution analysis
202 (Extended Data Fig. S1A).

203

204 Concerning samples with the highest transcript other than insulin, these were not noteworthy
205 different from the other samples in any of the clinical parameters or anatomical part of the
206 pancreas the tissue originated from. Nine of them had *PRSS1* (coding for trypsin) as the most
207 enriched transcript, pointing to exocrine contamination and one was marked by *MALAT1* and
208 was therefore excluded as suspect for cancerous cell contamination. The remaining samples
209 were remarkable for expressing a non-beta-cell endocrine gene, specifically 13 samples with
210 predominant alpha cell (*GCG* or *TTR*) and 18 samples with predominant gamma cell (*PPY*)
211 characteristic genes. This is partially reflected by the results of the deconvolution analysis
212 (Extended Data Figure S1). This specific group of 41 samples was not analyzed further since
213 the number of subjects in each of the four glycemic groups was too small for statistical analysis.

214

215 For both the “restricted” and the full data set, heatmaps of gene expression levels in the four
216 patient groups were prepared as a visual complement to the statistical analysis (Fig. 2B and
217 Extended Data Fig. S2A). Despite the marked differences between the findings in the
218 “restricted” and complete cohort, upregulation prevailed as the direction of gene dysregulation in
219 both of them (Fig. 2A and Extended Data Fig. S2A). Based on these observations, pancreatic
220 tissue sections of 5 ND and 5 T2D PPP with the “restricted” cohort were immunostained with
221 antibodies specific for histone H3 and H4 lysine acetylation – an epigenetic modification

222 associated with greater access of transcription factors to promoter sites resulting in increased
223 gene expression. Notably, qualitative assessment by immunostaining indicated a remarkable
224 increase of the signals for acetylated H3 and H4 in the islets, and also in the surrounding
225 exocrine cells of T2D PPP, compared to ND PPP (Fig. 2D).

226 Gene pathways are progressively perturbed from IGT to T2D

227
228 We further analyzed differentially expressed gene functions by gene set enrichment analysis
229 using Gene Ontology terms and KEGG pathways (Fig. 2C, Extended Data Fig. S2B and
230 Supplementary Tables 5 and 6). Results obtained from the different gene set collections cross-
231 validated each other, since similar biological themes emerged. Islets of pre-diabetic and diabetic
232 subjects displayed upregulation of islet genes that were functionally related to cell-extracellular
233 matrix interaction, immune response and signaling pathways, while expression of genes related
234 to RNA processing, protein translation and mitochondrial oxidative phosphorylation were
235 downregulated. Importantly, the analysis performed on the "restricted" cohort, differently from
236 the full dataset, also revealed that the strength of the enrichment increased with progression of
237 the disease (Fig. 2C and Extended Data Fig. S2B). These data suggest that early dysregulation
238 of gene pathways exacerbates with the decline of beta cell function.

239 WGCNA identifies islet gene modules correlated with HbA1c

240
241 To globally interpret transcriptomic data and identify sets of genes likely to be functionally
242 related and co-regulated, we grouped genes based on similarities in their expression profiles
243 into modules using a network-based approach²³. In the cohort of 133 PPP, we identified 36 co-
244 expressed gene modules, which were arbitrarily labeled M1 through M36. The expression
245 profiles of the genes in each module were summarized by a module eigengene, or first principal
246 component of the expression matrix. Module eigengenes were used to computationally relate

247 modules to one another and to genes or clinical variables. Correlation between module
248 eigengenes and diabetes-related clinical traits revealed modules M9 and M14 as those with the
249 highest positive and negative correlation with HbA1c, respectively (Fig. 3A and Supplementary
250 Table 7). The former consisted of a set of genes that showed similar patterns of increased
251 expression in most PPP with T2D (Fig. 3B), while the latter was mostly composed of genes with
252 coordinated down-regulation in diseased subject samples (Fig. 3C).

253

254 We next correlated the expression values of each gene contained in a module to the eigengene
255 of the module. The correlation coefficient from this calculation is denoted as the "module
256 membership" of the gene and serves as a quantitative measure of how representative a gene is
257 of the module it belongs to. Strong module memberships point to genes that are highly
258 connected in the underlying gene-gene similarity network of the WGCNA. This analysis allowed
259 us to identify highly connected genes or "hub" genes for HbA1c-related modules (Fig. 3D-E).
260 These included genes that we had previously identified as differentially expressed in subjects
261 with T2D, and which were correlated with HbA1c either positively, such as module M9 genes
262 *ALDOB* (FC=8.45 with adj. $p < 0.001$ in T2D vs. ND in the "restricted" cohort) and *FAIM2*
263 (FC=7.11 with adj. $p < 0.001$ in T2D vs. ND in the "restricted" cohort) or negatively, such as
264 module M14 genes *SLC2A2* (FC=-2.77 with adj. $p < 0.001$ in T2D vs. ND in the "restricted"
265 cohort) and *TMEM37* (FC=-1.73 with adj. $p < 0.001$ in T2D vs. ND in the "restricted" cohort). As in
266 other studies in mouse models of diabetes²⁴, we found *ALDOB* to be also upregulated in islets
267 from 13-week-old diabetic *db/db* mice compared to the heterozygous *db/+* littermate (Extended
268 Data Fig. S3A) as well as in a mouse beta, but not alpha, cell line upon exposure to high
269 glucose (Extended Data Fig. S3B). However, the overexpression of *ALDOB* in beta cells of T2D
270 PPP could not be verified by immunofluorescence on tissue sections due to the cross-reactivity
271 of the only available "specific" anti-ALDOB antibody with other aldolase isoforms (Extended
272 Data Fig. S3C).

273

274 The islet proteome is more heterogeneous in T2D

275

276 To verify and extend the transcriptomic data at the functional level of proteins, we analyzed the
277 mass spectrometry (MS)-based proteomic profiles of LCM pancreatic islets from five ND and
278 five T2D PPP (Supplementary Table 8). We chose these samples primarily based on tissue
279 availability and secondarily based on the levels of *ALDOB* found in RNA sequencing. Their islet
280 transcriptomics profiles closely resembled the one of the complete cohort: top regulated genes
281 in these 10 samples from T2D and ND PPP (Supplementary Table 2 and Extended Data Figure
282 S4C) were also among the most significantly differentially expressed islet genes in the entire
283 cohort. Using a very high sensitivity workflow on a novel trapped-ion mobility Time of Flight
284 mass spectrometer and miniaturized sample preparation²⁵, we identified 2,237±499 islet
285 proteins for ND PPP and 1,819±412 islet proteins for T2D PPP (Figure 4A). Quantitative
286 reproducibility between biological replicates was high with Pearson correlations ranging from
287 0.83 to 0.95 (Extended Data Fig. S4A). Principal component analysis (PCA) clustered the data
288 into two distinct groups matching the clinical stratification (Fig. 4B, see methods for detailed
289 data processing steps). Interestingly, islets of ND PPP clustered closely, indicating a very
290 similar proteome signature, while those of T2D PPP revealed substantial proteome
291 heterogeneity among each other. Differential expression analysis confirmed that islets of T2D
292 and ND PPP have very different proteomic profiles. The main differential drivers are well-
293 characterized markers of pancreatic islet cells, including *SLC2A2*²⁶, and many proteins
294 implicated in mitochondrial structure, translation, energy supply and amino acid or fatty
295 metabolism such as *YMEL1*, *MRPL12*, *BA3(C14orf159)*, *ACADS* and its paralogue *ACADSB*,
296 which were highly depleted in islets of T2D PPP (Fig. 4C). Besides *AKR7L*, *ACADS* was the
297 only other upregulated and differentially expressed gene in islets of both IGT and T2D PPP,
298 while being also downregulated at the protein level. All differentially expressed mitochondrial

299 proteins are encoded by the nuclear genome (Fig. S4B). Intriguingly, the level of the
300 sulfonylurea receptor ABCC8 subunit²⁷ was also strongly reduced in islets of T2D PPP. This
301 downregulation might be an effect secondary to pharmacological treatment, as three among
302 these patients had been treated with anti-diabetic SUR1 antagonists glibenclamide (DP197),
303 glimepiride (DP118) or mitiglinide (DP087) (Extended Data Fig. S4C). Furthermore, we found
304 that transcriptome and proteome levels of pancreatic islets from the same donors are very
305 different (Extended Data Fig. S4D), as shown in another cellular system at single-cell level²⁸.
306 Nevertheless, we report the glycolytic enzyme ALDOB to be consistently upregulated
307 (Proteome: 4-fold, Transcriptome: FPKM: 76.16 ± 50.82 in T2D PPP vs. 4.63 ± 0.95 in ND PPP),
308 and the glucose transporter SLC2A2 to be downregulated (Proteome: 4-fold, Transcriptome: 4-
309 fold) in islets of T2D vs. ND PPP samples on both modalities (Extended Data Fig. S4E, 4C).
310 This is consistent with our transcriptomic data and that of previous studies^{14,15} and our current
311 WGCNA analyses. Other proteins robustly overexpressed in islets of T2D PPP included the
312 alpha-L-fucosidase FUCA1 and the surface marker for hematopoietic stem cells THY1.

313

314 Next, we employed the proteomic ruler algorithm and annotations of subcellular localization to
315 compare the protein mass distribution of major cellular compartments²⁹(Fig. 4D). Islets of T2D
316 PPP lost an estimated protein mass of 6% in the Golgi apparatus, 24% in the endoplasmic
317 reticulum, and 27% in the mitochondria compared to those of ND PPP, while the cytoskeleton
318 protein mass was unchanged. Unsupervised hierarchical clustering of all 2,622 detected
319 proteins, clustered the data according to clinical categories (Fig. 4E). One-dimensional gene
320 ontology enrichment³⁰ revealed that two distinct clusters whose protein intensity levels
321 associated with the terms 'membrane attack complex' ($p < 2.18E-04$) and 'Immunoglobulin C-
322 domain' ($p < 2.68E-06$) were enriched by 2.27-fold and 2.36-fold in islets of T2D vs. ND PPP,
323 respectively. Proteins with the gene ontology-term 'differentiation' ($p < 3.09E-04$) and
324 'mitochondrion' ($p < 2.19E-08$) were expressed 1.65 and 1.78-fold in islets of ND PPP.

325 Plasma phospho- and sphingo-lipid trends are opposite in T2D

326
327 Our study encompassed two independently generated lipidomics data sets. First, shotgun
328 lipidomics was performed on peripheral blood plasma samples of the aforementioned cohort (4
329 ND, 21 IGT and IFG, 13 T3cD and 17 T2D) (Supplementary Tables 9 and 10). Second,
330 sphingolipid profiling was performed on peripheral blood samples of subjects within the cohort
331 subjected to transcriptomic analysis (11 ND, 32 IGT and IFG, 26 T3cD and 32 T2D)
332 (Supplementary Tables 11 and 12). Prior to data analysis, lipidomics samples from PPP with
333 very high bilirubin values ($>100 \mu\text{mol/l}$) were removed to avoid bias in lipidomics profiles. In
334 each of the two data sets, all available samples from non-diabetic PPP (ND, as previously
335 defined) and the subset of IGT PPP with $\text{HbA1c} < 6.0$ were combined into one group, which is
336 referred henceforth as ND for readability. The resulting sample sizes used in patient group
337 comparisons were as follows: 17 ND, 13 T3cD and 17 T2D in the shotgun lipidomics data set;
338 32 ND, 21 T3cD and 27 T2D in the targeted lipidomics data set.

339
340 Statistical tests included covariates to adjust for age, sex and BMI, similar to the transcriptomics
341 analysis. Pairwise comparisons of T2D vs ND and T3cD vs ND were performed. In shotgun
342 lipidomics, 113 lipid species from 11 classes were included in the data analysis. When
343 comparing T2D and T3cD to ND PPP, the majority of lipid classes displayed a remarkably
344 homogeneous downward-trend of the individual lipid species they comprised (Fig 5A-B). Most
345 prominently, plasma concentrations of lipids within the class of ether-linked
346 phosphatidylcholines (PC O-), a large class with 30 measured species, were lower in T2D
347 versus ND PPP. Fourteen lipids of this class were significantly decreased (adjusted $p < 0.05$),
348 with all of them showing at least a 1.4-fold change. A few lipid species from smaller
349 phospholipid classes (one phosphatidylcholine (PC), one lysophosphatidylcholine (LPC) and
350 one phosphatidylinositol (PI)), as well as two from the sphingomyelin class (SM), were also

351 significantly less abundant in T2D than in ND PPP (PC 18:0;0/18:2;0: FC=-1.43, adj. $p=0.040$;
352 LPC 18:0;0: FC=-1.54, adj. $p=0.037$; PI 18:0;0/18:2;0: FC=-1.36, adj. $p=0.045$; SM 40:1;2:, FC=-
353 1.33, adj. $p=0.037$; SM 34:1;2:, FC=-1.24, adj. $p=0.04$). (Fig. 5A-B and Supplementary Table
354 13).

355
356 Next, we performed targeted sphingolipidomics on 14 distinct lipid species for accurate plasma
357 level estimation (ceramides, dihydroceramides and sphingoid bases) (Supplementary Table 16).
358 Plasma levels of ceramides d18:1/18:0 and d18:1/20:0 were increased in T2D compared to ND
359 PPP (Cer d18:1/18:0: FC=1.34, $p=0.02$; Cer d18:1/20:0: FC=1.22, $p=0.01$, without multiple
360 testing correction). A similar trend towards elevation in T2D vs ND PPP was also observed in
361 the two dihydroceramide species having the same chain lengths as these ceramides, although
362 one of the two falls below the p -value threshold of 0.05 (DH Cer d18:0/18:0: FC=1.44, $p=0.09$;
363 DH Cer d18:0/20:0: FC=1.35, $p=0.02$). Thus, in our data set, plasma concentrations of some
364 ceramides and their precursor dihydroceramides appear to increase simultaneously in T2D. Cer
365 d18:1/24:0, but not the corresponding dihydroceramide, was observed to move in the opposite
366 direction being lower in T2D (FC=-1.28, $p=0.017$). Notably, ceramides were identified by LC-MS
367 (see methods) and, independently, by shotgun FT-MS and both profiles matched. Regarding the
368 LC-MS/MS analysis, the parent ion selected for dihydroceramides identification and
369 quantification was the protonated ion (without water loss). In FT-MS, we observed no significant
370 water loss from the ceramide standards. We therefore have reasons to believe that we detected
371 dihydroceramides, but not deoxyceramides, which are isomeric of the water loss form of the
372 dihydroceramides.³¹

373 Data integration identifies pathways for islet dysfunction

374

375 To identify a multivariate molecular profile that explains diabetes progression in the PPP cohort,
376 we performed a large-scale integrative multi-omics analysis combining clinical data with islet
377 transcriptomics and plasma lipidomics. Integration of transcriptomics and lipidomics data in the
378 same model enables to weigh the relative importance of lipid and gene expression features in
379 relationship to a chosen clinical trait. Hence, we explored the relationship between gene co-
380 expression modules and plasma lipids by computing a consensus orthogonal partial least
381 square (consensus OPLS)^{32,33} model with HbA1c as the outcome. All three types of biological
382 data, namely gene co-expression modules, lipids from the shotgun analysis and sphingolipids
383 from the targeted analysis, contributed to the model (35%, 46.5% and 18.5%, respectively),
384 suggesting that they help to explain HbA1c levels in a complementary way. Among them,
385 different lipids and gene modules appear as the most relevant variables in the statistical
386 modelling of HbA1c levels (Fig. 6A, 6B and Supplementary Table 14). Importantly, the model
387 explained a large portion of data variance, highlighting a good fit with the experimental data (see
388 Methods for more details).

389
390 Among all considered biological data, the co-expression modules M1, M4, M8, M9, M30, M35
391 and M36 were the top predictive variables for high HbA1c levels, along with the two ceramide
392 species C20 and C18. TAGs were also contributing, although to a lesser extent (Fig 6A, right
393 hand side). Conversely, low levels of HbA1c were strongly related to the co-expression modules
394 M12 and M14 (Fig 6A, left hand side). However, the majority of the predominant predictors for
395 low HbA1c were lipid species, most importantly the PC O- class. This class was also found to
396 be lower in T2D compared to ND patient groups in differential abundance analysis, as shown in
397 Fig 5A. A number of SM, PI and PC lipid species were next in the importance ranking related to
398 low HbA1c, followed by the gene co-expression module M29. These results suggest that the
399 profile of patients with increased HbA1c is characterized by multiple molecular components,
400 some of which represent signals that were neither captured by differential abundance analyses

401 comparing diabetes status groups nor by correlating gene co-expression modules individually to
402 HbA1c. Most importantly, consensus OPLS multi-omics analysis pointed towards additional
403 gene co-expression modules that may play a role in glucose dysregulation.

404

405 Next, we used the results from the integrative data modelling to infer a network of key altered
406 biological pathways in dysfunctional beta cells. To this end, we pooled gene modules positively
407 associated with HbA1c levels (M1, M4, M8, M9, M30, M35 and M36) (Fig. 6A) and assessed
408 their overlap to KEGG pathways by over-representation analysis. We found that the biological
409 themes underlying these genes were very similar to the pathways upregulated in T2D and IGT
410 PPP and include cell-matrix interaction, cell signaling and immune response (Fig. 6C and
411 Supplementary Table 15). The same strategy was used to identify pathways associated with
412 genes from modules with a negative prediction score for HbA1c (M12, M14 and M29) (Fig. 6A),
413 revealing an enrichment for metabolic pathways (Fig. 6C and Supplementary Table 15). Of
414 note, several islet genes differentially regulated in T2D PPP were driving the enrichment of
415 these pathways. These include, for example, *ALDOB*, which stood out for its strong correlation
416 to HbA1c levels (Fig. 3D and Fig. 6C). These genes, or the proteins encoded by them, should
417 be regarded as putative candidate biomarkers for monitoring disease progression and
418 therapeutic intervention.

419 Discussion

420

421 This study provides an extensive analysis on islets *in situ* and plasma samples from the largest
422 cohort of in-depth metabolically profiled living donors. Multi-omics data were generated using
423 state-of-the-art approaches and integrated in a fashion not previously used in studies on islet
424 dysregulation in relation to hyperglycemia in humans. Our transcriptomic and proteomic data
425 from islets *in situ* of ND subjects represent a valuable reference for future investigations. More

426 broadly, this dataset would be a worthwhile addition to the growing number of islet resources on
427 type 1 and type 2 diabetes by different consortia, such as the Network for Pancreatic Organ
428 Donors with Diabetes (nPOD)³⁴, Human Pancreas Analysis Program (HPAP)³⁵, or the
429 Translational human pancreatic Islet Genotype tissue - Expression Resource (TIGER)
430 (<https://www.t2dsystems.eu/tiger-database>). Furthermore, we could identify for the first time a
431 set of islet genes altered in their expression already in subjects with impaired glucose tolerance.
432 This, in turn, enabled us to acquire an unprecedented cross-sectional overview of the
433 progression of islet gene dysregulation in parallel with the continuous elevation of HbA1c
434 values, beyond conventional thresholds for clinical classification of patients.

435
436 Pathways involved in RNA biology and especially in mitochondrial function emerged to be most
437 negatively perturbed - a conclusion which in the case of the latter was strongly corroborated by
438 the proteomic analysis, which enabled the identification of known and unknown differentially
439 expressed proteins in islets of T2D PPP. In this context, we emphasize the downregulation of
440 mitochondrial ACADS and its paralogue ACADSB, which catalyze the beta oxidation of short-
441 chain fatty acids, including sodium butyrate. This finding is intriguing in view of the ability of this
442 metabolite to broadly upregulate gene expression through inhibition of histone deacetylases.
443 Unlike in previous studies on isolated islets from brain-dead organ donors^{14,19}, but similar to
444 previous studies by us in human¹⁴ and mouse models of diabetes³⁶ the vast majority of
445 differentially expressed genes in islets of T2D, but also IGT and T3cD PPP were upregulated.
446 Among those genes, *ALDOB* stands out being the one with the strongest correlation with the
447 islet gene module M9, which in turn has the strongest correlation with elevated HbA1c. Since
448 *ALDOB* is a marker of beta cell precursors³⁷, its overexpression could be interpreted as a sign
449 that in T2D, mature beta cells revert back to an immature stage of differentiation, or that a
450 compartment equivalent to the lifelong niche of virgin beta cells identified in adult mice expands
451 as a potential compensatory source of new beta cells³⁷. However, no additional disallowed gene

452 of immature beta cells, markers of beta cell precursors or other islet cell types were differentially
453 regulated, while key determinants of mature beta cells, such as *PDX1*, *MAFA*, *NKX6.1* or *UCN3*
454 were unchanged, at least at the transcriptomic level. Retention of fractions of major islet cell
455 types (alpha, beta and delta) within the islet in T2D, consistent with recent imaging studies in
456 samples from pancreatectomized subjects (Cohrs et al)¹⁷, was confirmed by deconvolution
457 analysis. Our global unbiased proteomic analysis, which corroborated the upregulation of
458 ALDOB, further showed that the expression profile of islet cells in T2D PPP is very divergent,
459 opposite to its remarkable homogeneity in islet cells of ND subjects. Hence, the regression of
460 beta cells toward a de-differentiated state following a linear trajectory recapitulating their
461 developmental path to maturation or their transdifferentiation into other islet cell types seems
462 less likely than a disharmonic relaxation of constraints on gene expression. Such processes,
463 although possibly reversible, could perturb the coordinated operation of islet cells, including beta
464 cells. In line with this, Lawlor *et al.* reported no evidence of beta cell
465 dedifferentiation/transdifferentiation and alterations in fractions of islet cells in the context of T2D
466 upon sequencing of single islet cells from a small cohort of ND and T2D organ donors, although
467 this conclusion has been more recently challenged³⁸. While we strived to selectively enrich the
468 beta cell content of our omics data by laser capture microdissection of bulk islets based on the
469 lipofuscin-associated autofluorescence of beta cells and by subsequent deconvolution of the
470 data during their analysis, the unavoidable presence of other cell types in the samples
471 introduces a degree of uncertainty. Thus, for the future it would be important to assess whether
472 overexpression of ALDOB occurs indeed in beta cells and if it affects their glycolysis and
473 metabolism, taking into account that its paralogue ALDOA, whose RNA and protein levels were
474 unchanged, remains by far the predominant islet aldolase species. Attention may also be
475 directed toward understanding whether impaired oxidative phosphorylation, as a likely outcome
476 of the massively decreased expression of mitochondrial proteins, and thus energy balance
477 homeostasis, accounts, at least in part, for the observed less restrained gene expression.

478

479 The transcriptome and proteome of islets from subjects with T2D displayed the occurrence of an
480 immune response. At this time, however, we are not aware of factors which might readily
481 account for the presence of such signals. Specifically, patients with antibodies against known
482 autoantigens of T1D were excluded from the analysis. As in a previous report¹⁵, histological
483 examination of the specimens did not reveal insulinitis or macrophage infiltration. Pancreatitis was
484 more common among subjects with normoglycemia (22%) than with T2D (15%). The presence
485 of cancer cells in our islet preparations is also unlikely. Specifically, a qualified pathologist
486 routinely examined the surgical specimen to minimize the chance of contamination by
487 neoplastic tissue before it was taken for downstream processing. Histological survey of the
488 tissue did not reveal the presence of neoplastic cells in the islets. The transcriptomic analysis in
489 a previous study indicated that exocrine contamination of LCM islets from PPP was comparable
490 or less than in the case of enzymatically-isolated islets from organ donors (OD)¹⁴. Moreover, in
491 the same study we found no evidence for an enrichment of tumor cell transcripts in LCM islets
492 of PPP compared to islets of OD. Likewise, an enrichment analysis of pancreatic cancer specific
493 genes in the differentially expressed islet gene sets reported here using hypergeometric test
494 showed no enrichment for any of the four described pancreatic cancer subtypes ($p = 0.87$) as
495 reported in Bailey et al 2016³⁹. Rather, the gene expression clustering was driven by the islet
496 isolation method and not by the origin of the tissue (OD vs. PPP). We still appreciate that in our
497 cohort cancer prevalence was higher in the T2D (69%) than in the ND (50%) group. Thus, we
498 cannot entirely rule out a metabolic pro-inflammatory impact of the cancer on islet gene and
499 protein expression or function.

500

501 Our lipidomics analyses revealed lowered phospholipid species (14 PC O-, one PC, one LPC,
502 one PI) and some elevated ceramides and dihydroceramides in T2D PPP. These findings match
503 observations reported in other recent studies on larger cohorts. Huynh et al (2019)⁴⁰ presented

504 a comprehensive shotgun lipidomics study on the AusDiab cohort, including 640 samples and
505 636 lipid species. In this work, many PC, PC O-, LPC and PI had a significant negative
506 association with blood glucose levels either after overnight fasting or at the 2-hour point of an
507 OGTT, including nine species that were found negatively associated with T2D in our own study
508 (PC 18:2;0/18:2;0, LPC 18:0;0, PI 18:0;0/18:2;0 and six PC O- species). In the same study, the
509 ceramide Cer d18:1/18:0 and its precursor DH Cer d18:0/18:0 had both a significant positive
510 association with fasting glucose, supporting our notion that this lipid pair might be linked to
511 diabetes status. Furthermore, several prospective case-control studies reported significantly
512 decreased PC, PC O- and LPC plasma concentrations⁴¹ or elevated dihydroceramide levels^{42,43}
513 in progressors to T2D compared to non-diabetic controls. The congruency of these results
514 points to these lipids as potential biomarkers of beta cell function in T2D.

515

516 Finally, we use a data fusion method^{32,33} to generate a model of how different molecular
517 features (islet gene co-expression, plasma shotgun lipidomics and targeted sphingolipidomics)
518 contribute to HbA1c levels in a continuum from healthy individuals to those with overt T2D. This
519 model allowed us to measure the *relative* importance of different molecular components in
520 explaining HbA1c variability, providing unique insights into the molecular profiles of individuals
521 as they lose glycemic control towards development of T2D. The rationale for combining plasma
522 lipidomics with islet gene expression data was that the levels of some plasma lipids may affect
523 pancreatic islets and/or reflect changes occurring within them and thus be useful as biomarkers
524 to assess beta cell dysfunction in prediabetes and T2D. To our knowledge this is the first time
525 such an approach has been used in this field and we suggest that, by modelling multiple levels
526 of information at the same time in deeply phenotyped populations such as the one presented
527 here, we can gain a holistic view of the system and draw conclusions regarding key pathways,
528 targets and biomarkers in metabolic and other diseases.

529 Data availability

530 RNA Sequencing data was deposited in the NCBI Gene Expression Omnibus with GEO
531 accession number GSE164416. Human genome reference assembly GRCh38 is publicly
532 available.

533 The proteomics raw datasets and the MaxQuant output files generated and analyzed throughout
534 this study were deposited at the ProteomeXchange Consortium via the PRIDE partner
535 repository with the project accession number PXD022561 (<https://www.ebi.ac.uk/pride/archive/>).

536 Lipidomics data was deposited in the Zenodo database (zenodo.org,
537 doi:10.5281/zenodo.4716063).

538 Acknowledgements

539 We wish to thank Leif Groop, Emma Ahlqvist, Stephan Speier, Triantafyllos Chavakis, Raphael
540 Scharfmann and Andrej Schevchenko for discussion; Sylvain Pradervand for advice on RNA-
541 Seq processing and QC; Corinne Rocher for Bioinformatics analysis support; Katja Pfriem for
542 administrative assistance. This project has received funding from the Innovative Medicines
543 Initiative 2 Joint Undertaking under grant agreement No 115881 (RHAPSODY). This Joint
544 Undertaking receives support from the European Union's Horizon 2020 research and innovation
545 program and EFPIA. This work is further supported by the Swiss State Secretariat for
546 Education, Research and Innovation (SERI) under contract number 16.0097-2. Work in the
547 Solimena lab is also supported with funds from the German Ministry of Education and Research
548 to the German Center for Diabetes Research (DZD). The opinions expressed and arguments
549 employed herein do not necessarily reflect the official views of these funding bodies.

550

551 Author contributions

552 J.W. and M.D., patient recruitment and surgery, provision of clinical data; E.S., N.K. and D.F.,
553 sample collection and processing, data entry; D.A., pathology; M.B., N.K. and E.S., patient
554 database management and selection; A-D.B. and M.M., proteomics; M.L., A.D., RNA
555 sequencing, C.L.Q., P.B.S.H, P.D., C. K., M. G., K.S., lipidomics and sphingolipidomics; L.W.,
556 M.B., A-D.B., F.Ma., F.Me., F.B. and Ca.K., analysis and integration of multi-omics data; E.B.,
557 autoantibody test; A.S., data in mouse tissue and cell lines; M.B., immunofluorescence stainings
558 and antibody validation; B.T., D.A., J.W., A.S., M.M., M.I. and M.S., conceptual insights and
559 provision of funds; L.W., M.B., A-D.B., F.Ma., F.Me., A.S., M.I., M.M. and M.S., writing of the
560 manuscript. All authors read, revised and approved the final version of the manuscript.

561 Competing interests

562 KS is CEO of Lipotype GmbH. KS and CK are shareholders of Lipotype GmbH. MJG is an
563 employee of Lipotype GmbH. PBSH and PD are employees of Servier. AS is an employee of
564 Sanofi-Aventis Deutschland GmbH. The other authors declare no conflict of interest.

565 References

- 566 1. Saeedi, P. *et al.* Global and regional diabetes prevalence estimates for 2019 and
567 projections for 2030 and 2045: Results from the International Diabetes Federation
568 Diabetes Atlas, 9th edition. *Diabetes Res. Clin. Pract.* **157**, (2019).
- 569 2. Mizera, M. *et al.* Type 2 Diabetes Remission 5 Years After Laparoscopic Sleeve
570 Gastrectomy: Multicenter Cohort Study. *Obes. Surg.* 1–7 (2020). doi:10.1007/s11695-
571 020-05088-w
- 572 3. Lim, E. L. *et al.* Reversal of type 2 diabetes: Normalisation of beta cell function in
573 association with decreased pancreas and liver triacylglycerol. *Diabetologia* **54**, 2506–
574 2514 (2011).

- 575 4. Talchai, C., Xuan, S., Lin, H. V., Sussel, L. & Accili, D. Pancreatic β cell dedifferentiation
576 as a mechanism of diabetic β cell failure. *Cell* **150**, 1223–1234 (2012).
- 577 5. Wang, Z., York, N. W., Nichols, C. G. & Remedi, M. S. Pancreatic β cell dedifferentiation
578 in diabetes and redifferentiation following insulin therapy. *Cell Metab.* **19**, 872–882
579 (2014).
- 580 6. Cinti, F. *et al.* Evidence of β -Cell Dedifferentiation in Human Type 2 Diabetes. *J. Clin.*
581 *Endocrinol. Metab.* **101**, 1044–1054 (2016).
- 582 7. American Diabetes Association. Classification and diagnosis of diabetes: Standards of
583 Medical Care in Diabetes-2020. *Diabetes Care* **43**, S14–S31 (2020).
- 584 8. Barovic, M. *et al.* Metabolically phenotyped pancreatectomized patients as living donors
585 for the study of islets in health and diabetes. *Molecular Metabolism* (2019).
586 doi:10.1016/j.molmet.2019.06.006
- 587 9. Poitout, V. *et al.* A call for improved reporting of human islet characteristics in research
588 articles. *Diabetes* **68**, 209–211 (2019).
- 589 10. Ebrahimi, A. *et al.* Evidence of stress in β cells obtained with laser capture
590 microdissection from pancreases of brain dead donors. *Islets* **9**, 19–29 (2017).
- 591 11. Toyama, H., Takada, M., Suzuki, Y. & Kuroda, Y. Activation of macrophage-associated
592 molecules after brain death in islets. *Cell Transplant.* **12**, 27–32 (2003).
- 593 12. Negi, S. *et al.* Analysis of Beta-Cell gene expression reveals inflammatory signaling and
594 evidence of dedifferentiation following human islet isolation and culture. *PLoS One* **7**, 1–
595 11 (2012).
- 596 13. Weir, G. C. Glucolipotoxicity, β -cells, and diabetes: The emperor has no clothes.
597 *Diabetes* **69**, 273–278 (2020).
- 598 14. Solimena, M. *et al.* Systems biology of the IMIDIA biobank from organ donors and
599 pancreatectomised patients defines a novel transcriptomic signature of islets from
600 individuals with type 2 diabetes. *Diabetologia* **61**, 641–657 (2018).

- 601 15. Gerst, F. *et al.* The Expression of Aldolase B in Islets is Negatively Associated with
602 Insulin Secretion in Humans. *J. Clin. Endocrinol. Metab.* **103**, 4373–4383 (2018).
- 603 16. Khamis, A. *et al.* Laser capture microdissection of human pancreatic islets reveals novel
604 eQTLs associated with type 2 diabetes. *Mol. Metab.* **24**, 98–107 (2019).
- 605 17. Cohrs, C. M. *et al.* Dysfunction of Persisting β Cells Is a Key Feature of Early Type 2
606 Diabetes Pathogenesis. *Cell Rep.* **31**, (2020).
- 607 18. Viñuela, A. *et al.* Genetic variant effects on gene expression in human pancreatic islets
608 and their implications for T2D. *Nat. Commun.* **11**, (2020).
- 609 19. Mahajan, A. *et al.* Fine-mapping type 2 diabetes loci to single-variant resolution using
610 high-density imputation and islet-specific epigenome maps. *Nat. Genet.* **50**, 1505–1513
611 (2018).
- 612 20. Taneera, J. *et al.* Identification of novel genes for glucose metabolism based upon
613 expression pattern in human islets and effect on insulin secretion and glycemia. *Hum.*
614 *Mol. Genet.* **24**, 1945–1955 (2014).
- 615 21. Carrat, G. R. *et al.* Decreased STARD10 Expression Is Associated with Defective Insulin
616 Secretion in Humans and Mice. *Am. J. Hum. Genet.* **100**, 238–256 (2017).
- 617 22. Xin, Y. *et al.* RNA Sequencing of Single Human Islet Cells Reveals Type 2 Diabetes
618 Genes. *Cell Metab.* **24**, 608–615 (2016).
- 619 23. Langfelder, P. & Horvath, S. WGCNA: An R package for weighted correlation network
620 analysis. *BMC Bioinformatics* **9**, 559 (2008).
- 621 24. Haythorne, E. *et al.* Diabetes causes marked inhibition of mitochondrial metabolism in
622 pancreatic β -cells. *Nat. Commun.* **10**, (2019).
- 623 25. Meier, F. *et al.* Online parallel accumulation–serial fragmentation (PASEF) with a novel
624 trapped ion mobility mass spectrometer. *Mol. Cell. Proteomics* **17**, 2534–2545 (2018).
- 625 26. Thorens, B. GLUT2, glucose sensing and glucose homeostasis. *Diabetologia* **58**, 221–
626 232 (2015).

- 627 27. Pipatpolkai, T., Usher, S., Stansfeld, P. J. & Ashcroft, F. M. New insights into KATP
628 channel gene mutations and neonatal diabetes mellitus. *Nature Reviews Endocrinology*
629 **16**, 378–393 (2020).
- 630 28. Brunner, A. D. *et al.* Ultra-high sensitivity mass spectrometry quantifies single-cell
631 proteome changes upon perturbation. *bioRxiv* 2020.12.22.423933 (2020).
632 doi:10.1101/2020.12.22.423933
- 633 29. Wiśniewski, J. R., Hein, M. Y., Cox, J. & Mann, M. A 'proteomic ruler' for protein copy
634 number and concentration estimation without spike-in standards. *Mol. Cell. Proteomics*
635 **13**, 3497–3506 (2014).
- 636 30. Cox, J. & Mann, M. 1D and 2D annotation enrichment: a statistical method integrating
637 quantitative proteomics with complementary high-throughput data. *BMC Bioinformatics*
638 **13 Suppl 16**, (2012).
- 639 31. Zitomer, N. C. *et al.* Ceramide synthase inhibition by fumonisin B1 causes accumulation
640 of 1-deoxysphinganine. A novel category of bioactive 1-deoxysphingoid bases and 1-
641 deoxydihydroceramides biosynthesized by mammalian cell lines and animals. *J. Biol.*
642 *Chem.* **284**, 4786–4795 (2009).
- 643 32. Boccard, J. & Rutledge, D. N. A consensus orthogonal partial least squares discriminant
644 analysis (OPLS-DA) strategy for multiblock Omics data fusion. *Anal. Chim. Acta* **769**, 30–
645 39 (2013).
- 646 33. Boccard, J. & Rutledge, D. N. Iterative weighting of multiblock data in the orthogonal
647 partial least squares framework. *Anal. Chim. Acta* **813**, 25–34 (2014).
- 648 34. Campbell-Thompson, M. *et al.* Network for Pancreatic Organ Donors with Diabetes
649 (nPOD): Developing a tissue biobank for type 1 diabetes. *Diabetes. Metab. Res. Rev.* **28**,
650 608–617 (2012).
- 651 35. Kaestner, K. H., Powers, A. C., Najj, A. & Atkinson, M. A. NIH initiative to improve
652 understanding of the pancreas, islet, and autoimmunity in type 1 diabetes: The Human

- 653 Pancreas Analysis Program (HPAP). *Diabetes* **68**, 1394–1402 (2019).
- 654 36. Ebrahimi, A. G. *et al.* Beta cell identity changes with mild hyperglycemia: Implications for
655 function, growth, and vulnerability. *Mol. Metab.* **35**, (2020).
- 656 37. van der Meulen, T. *et al.* Virgin Beta Cells Persist throughout Life at a Neogenic Niche
657 within Pancreatic Islets. *Cell Metab.* **25**, 911-926.e6 (2017).
- 658 38. Avrahami, D. *et al.* Single-cell transcriptomics of human islet ontogeny defines the
659 molecular basis of β -cell dedifferentiation in T2D. *Mol. Metab.* **42**, (2020).
- 660 39. Bailey, P. *et al.* Genomic analyses identify molecular subtypes of pancreatic cancer.
661 *Nature* **531**, 47–52 (2016).
- 662 40. Huynh, K. *et al.* High-Throughput Plasma Lipidomics: Detailed Mapping of the
663 Associations with Cardiometabolic Risk Factors. *Cell Chem. Biol.* **26**, 71-84.e4 (2019).
- 664 41. Suvitaival, T. *et al.* Lipidome as a predictive tool in progression to type 2 diabetes in
665 Finnish men. *Metabolism.* **78**, 1–12 (2018).
- 666 42. Wigger, L. *et al.* Plasma Dihydroceramides Are Diabetes Susceptibility Biomarker
667 Candidates in Mice and Humans. *Cell Rep.* **18**, 2269–2279 (2017).
- 668 43. Mamtani, M. *et al.* Lipidomic risk score independently and cost-effectively predicts risk of
669 future type 2 diabetes: Results from diverse cohorts. *Lipids Health Dis.* **15**, (2016).
- 670

671 Figure Legends

672 **Figure 1: Overview of the experimental procedures and cohort characteristics.** A)
673 Experimental procedures overview. Clinical data and peripheral blood were collected
674 preoperatively, and the snap-frozen surgical pancreatic tissue used for LCM of the islets of
675 Langerhans. Blood samples were analyzed for lipidomics, while LCM islets for transcriptomics
676 and proteomics. Omics datasets were individually evaluated in relationship to glycemic status
677 and further integrated with each other using Consensus Orthogonal Partial Least Squares

678 (OPLS) analysis. B) Waffle plot showing the structure of the cohort in terms of
679 glycemic/diabetes categories based on American Diabetes Association criteria. Absolute
680 numbers for each category are given in the legend boxes. C) Boxplots of four major clinical
681 parameters relevant for diabetes diagnosis and management. Statistically significant differences
682 from ND PPP were determined using the two-sided t-test ($*p<0.05$; $**p<0.01$). Boxplot spans
683 from 25th until 75th percentile, with centerline at median, whiskers extend to the most extreme
684 data point which is no more than 1.5 times the length of the box away from the box. Number
685 of observations in each comparison and category: age and BMI - 18 for ND, 41 for IGT($p=0.006$
686 and $p=3.792-4$), 35 for T3cD ($p=0.001$ and $p=0.003$) and 39 for T2D ($p=0.003$ and $p=0.005$);
687 fasting glycemia - 16 for ND, 38 for IGT ($p=2.936-6$), 34 for T3cD ($p=1.249-7$) and 33 for T2D
688 ($p=2.692-7$); glycemia at 2h point of OGTT: 15 for ND, 38 for IGT ($p=1.486-6$) and 23 for T3cD
689 ($p=3.111-11$).LCM: Laser Capture Microdissection; ND: Non-diabetic; IGT: Impaired Glucose
690 Tolerance; T3cD: Type 3c Diabetes; T2D: Type 2 Diabetes.

691 **Figure 2: Transcriptional changes between non-diabetic, pre-diabetic and diabetic**
692 **patients.** A) Number of DE genes identified by comparing glycemic groups of PPP in the entire
693 (all samples) or "restricted" cohort (*INS* filtered), using linear model with age, sex and BMI as
694 covariates. B) Gene expression profile of DE genes in the "restricted" cohort. Columns
695 represent patients grouped according to their glycemic status and ordered based on increasing
696 HbA1c levels. Rows, representing DE genes (variance stabilizing transformation normalized
697 counts), were clustered based on Euclidean distance. The colored side bar indicates in which
698 comparisons a gene was identified as differentially expressed. C) Gene Set Enrichment
699 Analysis of DE genes between IGT, T3cD or T2D and ND PPP in the "restricted" cohort. GO
700 terms and KEGG pathways are colored according to the normalized enrichment score.
701 Corresponding p-values are also indicated ($*p<0.05$, $**p<0.01$). D) Immunofluorescence for
702 insulin (green), acetylated histones H3 (left) and H4 (right) (magenta) in representative samples

703 of formalin fixed paraffin embedded pancreatic tissues from 5 ND and 5 T2D PPP. Scale bars
704 correspond to 20 μ m. DE: differentially expressed; ND: Non-diabetic; IGT: Impaired Glucose
705 Tolerance; T3cD: Type 3c Diabetes; T2D: Type 2 Diabetes.

706 **Figure 3: Identification of co-expressed gene modules related to diabetes traits.** A)
707 Correlation between module eigengenes and clinical traits including age, BMI, HbA1c, fasting
708 glucose, glucose at 2-hours after OGTT, HOMA2-B and HOMA2-IR. Each cell contains the
709 corresponding Spearman correlation coefficient and Student p value (in parenthesis). Cells are
710 colored according to their correlation to clinical traits. Modules are ordered based on their
711 correlation to HbA1c. B-C) Gene expression profiles of gene modules M9 (B) and M14 (C).
712 Columns, representing PPP, were grouped according to their glycemic status and ordered
713 based on increasing HbA1c levels. Rows, representing genes (variance stabilizing
714 transformation normalized counts), were clustered based on Euclidean distance. D-E) Scatter
715 plot of module membership vs. gene significance for HbA1c in modules M9 and M14. Genes
716 with the highest module membership and gene significance ("hub genes") are labeled. ND: Non-
717 diabetic; IGT: Impaired Glucose Tolerance; T3cD: Type 3c Diabetes; T2D: Type 2 Diabetes.

718 **Figure 4: Proteomics Analysis.** A) Number of identified proteins from pooled human
719 pancreatic islet cells isolated by LCM from PPP classified as non-diabetic (ND, N=5) or with
720 T2D (N=5). Boxplot spans from 25th until 75th percentile with centerline at median. Whiskers
721 extend to the most extreme data points in either direction. B) Principal Component Analysis
722 (PCA) of all grouped pancreatic islet measurements (ND=blue, T2D=orange). C) Volcano plot
723 comparing p values and \log_2 -fold changes between islets of ND and T2D PPP. Multiple
724 hypothesis testing is controlled via Benjamini Hochberg correction at 5% False discovery rate.
725 D) Percentage distribution of total protein islet mass and its contribution per organelle between
726 ND and T2D PPP. The ND/T2D islet protein mass ratio in different organelles was normalized
727 by the nucleus protein mass. E) Hierarchical clustering of all islet proteins identified in the T2D

728 and ND PPP clusters. Log₂-transformed intensity values were normalized by z-scoring before
729 the clustering followed by one-dimensional gene ontology enrichment for cellular compartment
730 and keywords for each of the clusters. Distribution of systematically enriched clusters is shown
731 as the geometric mean at 95% confidence interval for each respective term in non-diabetic (ND,
732 N = 5) and type 2 diabetics (T2D, N = 5) with centerline at the geometric mean with 95%
733 confidence interval.

734 **Figure 5: Lipidomics differential analysis.** A-B) Shotgun lipidomics covering a variety of lipid
735 classes: Ceramides (Cer), Diacylglycerols (DAG), Lysophosphatidylcholines (LPC),
736 Lysophosphatidylethanolamines (LPE), Phosphatidylcholines (PC), Ether-linked
737 Phosphatidylcholines (PC O-), Phosphatidylethanolamines (PE), Ether-linked
738 Phosphatidylethanolamines (PE O-), Phosphatidylinositols (PI), Sphingomyelins (SM),
739 Triacylglycerols (TAG). Volcano plots represent comparisons of plasma lipid levels between ND
740 and T2D PPP. The X-axis shows direction and magnitude of the change; the Y-axis represents
741 the statistical significance of the change. Each point is a lipid species, colored by lipid class to
742 highlight class-specific trends. C) Targeted lipidomics on dihydroceramides (DH Cer),
743 ceramides (Cer) and Sphingoid bases (SB). Each heatmap column represents the comparisons
744 of plasma levels between ND and T2D PPP. Heatmap colors represent direction and magnitude
745 of the change. Log₂ Fold Change: ratio of mean lipid concentration in the two groups, log₂
746 transformed. Statistical model used for all panels: linear regression with age, sex and BMI as
747 covariates (*p*: *p* value); adjustment of *p* values across all lipid species by the Benjamini-
748 Hochberg method (adj. *p*: adjusted *p* value). T2D: Type 2 Diabetes; T3cD: Type 3 Diabetes; ND
749 & PD: non-diabetic and pre-diabetic (with impaired fasting glucose and/or impaired glucose
750 tolerance) with HbA1c<6.0.

751 **Figure 6: Multiblock data modeling of HbA1c.** A) Bar plot showing the variable importance in
752 the multiblock consensus OPLS model. The Y-axis represents the importance scores for the

753 predictors multiplied by the sign of the loadings on the predictive latent variable. Variables with
754 importance in projection > 1.2 were selected. B) Statistical significance of the model through
755 permutation test. C) Network representation of functional pathways enriched in modules with
756 best prediction scores for HbA1c. Pathways are represented as gray nodes. Genes are
757 represented as nodes sized based on their correlation to HbA1c and colored based on their
758 differential expression in T2D vs. ND PPP. Only genes with significant differential expression
759 (adj. $p < 0.05$) in the "restricted" cohort are shown. VIP Variable Importance in Projection, DE:
760 Differentially expressed; ND: Non-diabetic, T2D: Type 2 Diabetes.

761

762 Material and methods

763 Cohort

764 Our cohort comprised 133 adult patients undergoing pancreatic surgery for a variety of
765 indications (benign and malignant neoplasms, chronic pancreatitis, pancreatic cysts etc.) from
766 the University Hospital Carl Gustav Carus Dresden who after informed consent participated in
767 this study over a period of 5 years. The study was conducted with the ethical approval of the
768 Ethical Committee of the Technische Universität Dresden. Based on the thresholds set by the
769 American Diabetes Association⁴ (ADA) for fasting glucose, HbA1c and 2-hour glycemia of an
770 oral glucose tolerance test (OGTT) in the days immediately before surgery 18 of these patients
771 were classified as non-diabetic (ND), 41 with impaired glucose tolerance (IGT), including 3 with
772 impaired fasting glucose (IFG) only, 35 with Type 3c Diabetes (T3cD) and 39 with Type 2
773 Diabetes (T2D). A diagnosis of T3cD was made whenever the occurrence of diabetes was not
774 recognized for longer than 1 year prior to the onset of the symptoms leading to surgery and the
775 subject was negative for the presence of circulating autoantibodies against pancreatic islets,
776 which were assessed as previously described¹¹. In all analyses IFG and IGT subjects were
777 merged in one group hereafter labeled as IGT PPP. Medical and family history and relevant
778 clinical biochemistry data available from the routine medical processing of the patients were
779 retrieved from the hospital database and referring physicians. Patients who underwent
780 neoadjuvant chemotherapy as well as those with endocrine neoplasms of the pancreas were
781 excluded from this study.

782 Human pancreatic tissue and peripheral blood processing

783 Surgical tissue specimens were examined by a certified pathologist immediately after resection
784 as per regular clinical procedures. Fragments of healthy pancreatic tissue from the resection
785 margins were excised, snap frozen in liquid nitrogen and stored at -80°C either natively or
786 embedded in TissueTek OCT compound. Estimated warm and cold ischaemia time was on

787 average 2 hours. Peripheral blood samples were stored at -80°C in aliquots of full blood, plasma
788 and serum.

789 Transcriptomics

790 Islet procurement and RNA isolation

791 Pancreatic tissue was sectioned in a cryostat and mounted on UV pre-treated Zeiss
792 MembraneSlide 1.0 PEN slides. Laser capture microdissection (LCM) was done with a Zeiss
793 Palm MicroBeam system using autofluorescence to identify islets, as previously described⁴⁴.
794 RNA was isolated from approximately 20x6µm³ of islet tissue using the Arcturus PicoPure RNA
795 Isolation Kit. Only preparations with RNA Integrity Number ≥5 were used for RNA sequencing.
796 The entire handling of the tissue samples was done in a strictly RNase free environment.

797 Library preparation, RNA Sequencing and alignment

798 Sequencing libraries were prepared from bulk RNA using the Illumina SmartSeq protocol. Single
799 ended 76bp sequencing was done with an Illumina HiSeq 2500 or Illumina HiSeq 500 at the
800 Next Generation Sequencing Core Facility of the CMCB Dresden, with the target depth of 35
801 million fragments per library. From FASTQ files, purity-filtered reads were trimmed with
802 Cutadapt to remove adapters and low-quality sequences (v. 1.8)⁴⁵. Reads matching to
803 ribosomal RNA sequences were removed with fastq_screen (v. 0.11.1)⁴⁶. Remaining reads
804 were further filtered for low complexity with reaper (v. 15-065)⁴⁷. Reads were aligned against
805 Homo sapiens GRCh38.92 genome using STAR (v. 2.5.3a)⁴⁸. The number of read counts per
806 gene locus was summarized with htseq-count (v. 0.9.1)⁴⁹ using Homo sapiens GRCh38.92 gene
807 annotation. Quality of the RNA-seq data alignment was assessed using RSeQC (v. 2.3.7)⁵⁰.

808 RNA Sequencing quality control, processing and differential expression analysis

809 RNA Sequencing datasets were screened for exocrine contamination in an initial quality control
810 (QC) step. Analysis of the absolute number of detected expressed genes, gene body coverage

811 and cumulative gene diversity assessment flagged a number of libraries to be of insufficient
812 quality for downstream analysis. Libraries were filtered for minimal expression by removal of
813 genes with less than 5 mean raw reads. Reads were normalized for library size and transformed
814 for variance stabilizing using tools from the DESeq2 Bioconductor package⁵¹. Further analysis
815 revealed 41 libraries in which transcripts other than insulin (*INS*) displayed the highest
816 normalized number of reads. Differential expression analysis across the clinical categories (ND,
817 IGT, T3cD, T2D) was performed using limma function with voom approach from the limma
818 Bioconductor package^{52,53} on both the full dataset of 133 libraries which passed the QC analysis
819 as well as on the "restricted" dataset of 92 libraries featuring *INS* as the highest expressed gene
820 based on the linear model with age, sex and BMI as covariates. All analysis pertaining
821 transcriptomic data was done on R platform (version 3.6.3).

822 Gene set enrichment analysis of differentially expressed genes

823 Functional enrichment analyses of differentially expressed genes in IGT, T2D or T3cD
824 compared to ND patients were performed by weighted gene set enrichment analysis (GSEA) on
825 unfiltered gene lists ranked by decreasing differential expression test statistics. Gene Ontology
826 (GO) term and Kyoto Encyclopedia of Genes and Genomes (KEGG) pathway collections were
827 restricted to gene sets with a minimum and maximum sizes of 100 and 500, respectively. The
828 enrichment scores were normalized by gene set size and their statistical significance was
829 assessed by permutation tests ($n=1,000$). GO enrichment analyses were carried out using the
830 gseGO function from the R package clusterProfiler (version 3.10.1)⁵⁴. GO terms enriched in at
831 least one comparison were identified using p value and normalized enrichment score thresholds
832 < 0.01 and > 2.5 , respectively. Redundancy of enriched GO terms was removed using the
833 clusterProfiler simplify function (selecting the most representative term by p value) and
834 enrichment maps generated using the emaplot function from the R package enrichplot (version
835 1.2.0). KEGG pathway enrichment analyses were performed using the clusterProfiler gseKEGG

836 function. Results were filtered based on a p value threshold < 0.01 and a normalized enrichment
837 score threshold > 2 . To simplify results visualization and interpretation, redundant KEGG
838 pathways were also collapsed into fewer biological themes using the enrichment map
839 visualizations.

840 Weighted Gene Correlation Network Analysis

841 Gene Co-expression Network Construction

842 The gene co-expression network was created following the weighted gene correlation network
843 analysis (WGCNA) protocol as implemented in the WGCNA package in R (version 1.68)²³, as
844 previously described¹⁴. WGCNA was performed on batch-corrected, normalized and variance
845 stabilizing transformed expression data from the full cohort of 133 subjects. The co-expression
846 network was constructed by calculating an adjacency matrix using Pearson correlation, pairwise
847 complete observations and unsigned method. The soft-threshold parameter was optimized with
848 the function `pickSoftThreshold` and the best threshold ($\alpha = 7$) selected by visual inspection. The
849 adjacency matrix was then computed into a topological overlap matrix (TOM), converted to
850 distances, and clustered by hierarchical clustering using average linkage clustering. Modules
851 were identified by dynamic tree cut using the hybrid method and parameters `minClusterSize=20`
852 and `deepSplit=2`. Similar modules were merged using a module eigengene distance of 0.15 as
853 the threshold.

854 Identification of co-expressed gene modules

855 We correlated the module eigengenes to clinical traits using Spearman correlation (pairwise
856 complete observations) and calculated the corresponding p values using the `cor` and
857 `corPvalueStudent` functions from the WGCNA package, respectively. Module-trait correlations
858 were represented as heatmap using the `labeledHeatmap` function from the WGCNA package.
859 The modules displaying the most positive or negative correlation to HbA1c were further

860 analysed. Normalized and variance stabilizing transformed gene counts for selected modules
861 were plotted as heatmap using the heatmap.2 function from the R gplots package (version
862 3.0.1.2). Rows (representing genes) were scaled and hierarchically clustered by Euclidean
863 distances. Columns, representing patients, were custom ordered as described in the legend of
864 figure 3. Module hub genes, such as highly connected genes within a module that could have a
865 strong influence on a phenotypic trait, were identified as those with highest correlations with the
866 particular trait and highest correlations with the module eigengene.

867 Significance of gene co-expression modules

868 We tested the significance of the co-expression modules by comparing their intramodular
869 connectivity (connectivity between nodes within the same module, as computed by the WGCNA
870 intramodularConnectivity function) to the background as follows. For each selected module of
871 size N, we calculated a Z-score as in equation 1:

$$872 \quad Z = (k - \mu) / \sigma \quad (1)$$

873 where k is the intramodular connectivity and μ and σ are the mean and standard deviation of the
874 intramodular connectivity from 1,000 randomly sampled modules of size N respectively.
875 Empirical p values were then calculated as the fraction of random intramodular connectivity
876 values \geq to the observed intramodular connectivity. For the modules with the highest variable
877 importance in projection score in the HbA1c multiblock model, all of the random intramodular
878 connectivity values were below the observed intramodular connectivity, suggesting that these
879 modules were more compact than modules assembled by randomly sampling the same number
880 of genes from the expression data (Supplementary Table 7).

881 Functional profiles of gene modules most predictive for HbA1c

882 The clusterProfiler enrichKEGG function was used to test for the over representation of selected
883 co-expressed gene modules in KEGG pathways using hypergeometric distribution. A p value
884 threshold < 0.01 was used to identify enriched terms. Enrichment map visualizations were used

885 to overcome gene set redundancy. Results were displayed as networks of enriched pathways
886 and overlapping genes using cytoscape (version 3.5.1).

887 Deconvolution analysis

888 In all samples a cell proportions matrix was produced using the R package DeconRNASeq
889 (v.1.26.0) on RPKM-transformed data. The signature file provided to DeconRNASeq comes
890 from Xin et al. (2016)²², Supplementary Table S2A, obtained using single-cell data. It was
891 adapted to the human genome version 38 by excluding 15 obsolete genes.

892 Lipidomics

893 894 Sample availability and sample overlap with transcriptomics data

895 Pre-operative plasma lipidomics samples were obtained from a subset of the PPP cohort.
896 Shotgun lipidomics analysis was performed on plasma from 55 PPP. These included 53
897 subjects who also had their islet transcriptomics profile included in this study plus two PPP who
898 were not part of the transcriptomics analysis because the RNA-Seq data failed to pass the
899 quality control. Moreover, targeted sphingolipid analysis was performed on plasma from 101
900 PPP. These included 98 PPP whose transcriptomics data was also included in this study plus
901 three PPP whose RNA-Seq data was excluded for quality reasons. The number of samples in
902 the two types of lipidomics analysis was smaller than in islet transcriptomic analysis because of
903 the limited availability of plasma samples. The 55 PPP with shotgun lipidomics data were a
904 subset of the 101 PPP with targeted sphingolipid data, with the difference in sample numbers
905 being determined by plasma sample availability as well.

906

907 Shotgun lipidomics measurements

908 A streamlined mass-spectrometry (MS) -based platform for shotgun lipidomics developed by
909 Lipotype GmbH (Dresden, Germany) was used for lipidomic profiling of patient plasma samples.
910 Lipid extraction, internal standard addition and infusion into the mass spectrometer were
911 performed as previously described⁵⁵. The internal standard mixture contained: cholesterol D6
912 (chol), cholesterol ester 20:0 (CE), ceramide 18:1;2/17:0 (Cer), diacylglycerol 17:0/17:0 (DAG),
913 phosphatidylcholine 17:0/17:0 (PC), phosphatidylethanolamine 17:0/17:0 (PE),
914 lysophosphatidylcholine 12:0, (LPC) lysophosphatidylethanolamine 17:1 (LPE), triacylglycerol
915 17:0/17:0/17:0 (TAG) and sphingomyelin 18:1;2/12:0 (SM).

916
917 Samples were analyzed by direct infusion in a QExactive mass spectrometer (Thermo
918 Scientific) in a single acquisition. Tandem mass-spectrometry (MS/MS) was triggered by an
919 inclusion list encompassing corresponding MS mass ranges scanned in 1 Da increments. MS
920 and MS/MS data were combined to monitor CE, DAG and TAG ions as ammonium adducts;
921 PC, PC O-, as acetate adducts; and PE, PE O- and PI as deprotonated anions. MS only was
922 used to monitor LPE as deprotonated anion; Cer, SM and LPC as acetate adducts and
923 cholesterol as ammonium adduct.

924 Data post-processing and normalization were performed using an in-house developed data
925 management system. Only lipid identifications with a signal-to-noise ratio >5 and a signal
926 intensity 5-fold higher than in corresponding blank samples were considered for further analysis.
927 The median coefficient of lipid subspecies variation (RSD), as accessed by the repeated
928 analysis of reference samples, was 7.5%.

929 Targeted sphingolipid measurements

930 Ceramides (C16:0 cer, C18:0 cer, C18:1 cer, C20:0 cer, C22:0 cer, C24:0 cer and C24:1 cer),
931 Dihydroceramides (C16:0 DHcer, C18:0 DHcer, C18:1 DHcer, C20:0 DHcer, C22:0 DHcer,
932 C24:0 DHcer, C24:1 DHcer) and precursors (Sphingosine, Sphinganine, 1-Deoxysphinganine, 1-

933 Methyldeoxysphinganine, SB) were quantified in plasma by liquid chromatography tandem
934 mass spectrometry (LC-MS/MS). In addition to samples, seven-point calibration curves and 3
935 levels of quality controls were made from pure standards in BSA 5%. Finally, reference plasma
936 spiked with analytes at two different levels were prepared as additional QC samples.

937 Lipid chromatographic separation was performed on a UPLC I-Class system (Waters) equipped
938 with an Acquity BEH C18, 100 x 2.1 mm, 1.7 µm column (Waters) heated at 60°C. Mobile phase
939 were A: 0.1 % (V/V) formic acid in water and B: 0.1 % (V/V) formic acid in acetonitrile/
940 isopropanol (60/40). Flow rate was set à 0.5 ml/min and a gradient was applied as follows:
941 0min: 45% A, 2min: 45% A, 3min: 15% A, 13min: 0% A, 14min: 45% A, 16 min: 45%A Mass.
942 Mass analysis was performed on an API 6500 system (Sciex) operating with an electrospray
943 source in positive mode. General parameters were set as follows: curtain gas: N₂ (35 PSI), Ion
944 source gas 1: Air (50 PSI), Ion source gas 2: Air (50 PSI), ion source voltage: 5500 V,
945 temperature: 300°C, collision gas: N₂ (7). Scheduled multiple reaction monitoring (MRM) mode
946 was used with a target scan time of 0.5s and an MRM detection window of 60s.

947

948 Data was acquired using Analyst 1.6.2 (Sciex) and data processing was performed with
949 MultiQuant 3.0 (Sciex). Peak area of analyte and internal standard were determined by the
950 MultiQuant 3.0 (Sciex) integration system. Analyte concentrations were determined using the
951 internal standard method. The standard curves were generated from the peak area ratios of
952 analyte/internal standard using linear regression analysis with 1/x² weighting (except for C24
953 cer: quadratic regression analysis). Quantifications of analytes were accepted based on quality
954 control samples. A tolerance of 25% and 30% was applied for accuracy and precision of QC
955 samples and spiked plasma samples, respectively. All concentrations were reported in ng/mL.
956 Internal standards used are listed in the Supplementary Table 16.

957 Analysis of shotgun lipidomics and targeted sphingolipid data

958 The statistical analyses of the shotgun lipidomics and targeted sphingolipid data sets were kept
959 separate. Identical analysis steps were applied to the two data sets. Both sets had missing data
960 values. Lipid species with $\geq 25\%$ missing values across all available plasma samples were
961 removed from the data set. This filtering resulted in 113 lipid species that were kept in the
962 shotgun data set (523 were removed) and 14 in the targeted data set (4 were removed). For the
963 lipids that remained in the data sets, missing values were imputed using a random forest
964 approach, applying the function `missForest` from the R package `missForest`, with default
965 parameters. In a next step, samples were filtered based on subject characteristics: individuals
966 with bilirubin levels $\geq 100 \mu\text{mol/l}$ were removed before all analysis; moreover, individuals
967 categorized as IGT with an $\text{HbA1c} \geq 6\%$ were excluded from the group comparisons in
968 differential analysis, but they were retained in other analyses involving lipidomics data. In
969 differential analysis, due to the limited number of available ND samples, the ND and the
970 included IGT samples were combined into a single group for comparison with other sample
971 groups, as described in the result section.

972

973 For differential analysis, linear models were applied, using the function `lm` from the R `stats`
974 package. For each comparison between two sample groups, a linear model that included
975 diabetes status as the main explanatory variable and age, sex and BMI as covariates was fitted
976 to the data from the two groups. P values for diabetes status were adjusted across all included
977 lipid species with the Benjamini-Hochberg method, separately for each comparison. In addition,
978 ANCOVA results from the three groups T2D, T3cD and ND (as defined above) with the same
979 covariates were computed, with p -value adjustment across all lipid species as well.

980 Integrative analysis of transcriptomics and lipidomics

981 Multiblock modeling

982 Consensus Orthogonal Partial Least Squares (OPLS) model was computed with the MATLAB 9
983 environment with combinations of toolboxes and in-house functions that are available at
984 <https://gitlab.unige.ch/Julien.Boccard/consensusopls>. Modified RV-coefficients were computed
985 with the publicly available MATLAB m-file⁵⁶. KOPLS-DA was assessed with routines
986 implemented in the KOPLS open source package⁵⁷. Consensus OPLS modeling was performed
987 on shotgun lipidomics, targeted sphingolipids and transcriptomics data tables, which were all
988 autoscaled prior to the analysis. The Consensus OPLS model distinguishes variation of data
989 that is correlated to Y response and those which is orthogonal to Y response. This eases the
990 biological interpretation of results and enables the link between variation of variables and
991 variation of the outcome while removing information coming from other sources of variation.
992 The model resulted in 3 components: 1 predictive latent variable and 2 orthogonal latent
993 variables. The quality of the model was assessed by R^2 and Q^2 values, which define the portion
994 of data variance explained by the model and the predictive ability of the model, respectively.
995 The predictive component carried 11% of the total explained variance of global data (R^2X) and
996 explained 51.7% of variation of HbA1c (R^2Y). This indicates that the model was able to explain a
997 large part of variation of the response variable based on the different data matrices. The Q^2
998 value was computed by a K-fold cross validation (K=7), which led to a goodness of prediction of
999 $Q^2 = 0.26$.

1000

1001 To ensure the validity of the model, a series of 1,000 permutation tests were carried out by
1002 mixing randomly the original Y response (HbA1c patient values). The true model Q^2 value was
1003 clearly distinguished and statistically different from the random models distribution ($p < 0.001$,
1004 mean = -0.1778, standard deviation (SD) = 0.150, n = 1,000). The variable relevance to explain the
1005 HbA1c variation was evaluated using the variable importance in projection (VIP) parameter,

1006 which reflects the importance of variables both with respect to the response and to the
1007 projection quality. The most relevant features were selected using a VIP threshold > 1.2.

1008 Proteomics

1009 Sample Preparation

1010 Pooled pancreatic islet cells with an approximate surface area of 80,000 μm^2 were collected via
1011 Laser Capture Microdissection (LCM) onto adhesive cap tubes. Isolates were reconstituted in a
1012 20 μl lysis buffer (PreOmics, Germany) and transferred into PCR tubes⁵⁸. Samples were boiled
1013 at 95°C for 1min to denature proteins and reduce and alkylate cysteines without shaking in a
1014 thermocycler (Eppendorf GmbH) followed by sonication at maximum power (Bioruptor,
1015 Diagenode, Belgium) for 10 cycles of 30sec sonication and 30sec cooldown each. Sample liquid
1016 was briefly spun down and boiled again for 10min without shaking. 20 μl of 100mM TrisHCl pH
1017 8.5 (1:1 v/v) and 20ng Trypsin/LysC were added to each sample, followed by overnight
1018 digestion at 30°C without shaking. The next day, 40 μl 99% Isopropanol 5% Trifluoroacetic acid
1019 (TFA) (1:1 v/v) was added to the solution and mixed by sonication. Samples were then
1020 subjected to stage-tip cleanup via styrenedivinylbenzene reversed-phase sulfonate (SDB-RPS).
1021 The sample liquid was loaded on one 14-gauge stage-tip plug. Peptides were cleaned up with
1022 2x200 μl 99% Isopropanol 5% TFA and 2x200 μl 99% ddH₂O 5% TFA in an in-house made
1023 Stage-tip centrifuge at 2,000xg, followed by elution in 40 μl 80% Acetonitrile, 5% Ammonia and
1024 dried at 45°C in a SpeedVac centrifuge (Eppendorf, Concentrator plus) according to the 'in-
1025 StageTip' protocol (PreOmics, Germany). Peptides were resuspended in 0.1% TFA, 2% ACN,
1026 97.9% ddH₂O.

1027 Liquid chromatography and mass spectrometry (LC-MS)

1028 LC-MS was performed with an EASY nanoLC 1200 (Thermo Fisher Scientific) coupled online to
1029 a trapped ion mobility spectrometry quadrupole time-of-flight mass spectrometer (timsTOF Pro,

1030 Bruker Daltonik GmbH, Germany) via nano-electrospray ion source (Captive spray, Bruker
1031 Daltonik GmbH). Peptides were loaded on a 50cm in-house packed HPLC-column (75µm inner
1032 diameter packed with 1.9µm ReproSil-Pur C18-AQ silica beads, Dr. Maisch GmbH, Germany).
1033 Sample analytes were separated using a linear 120min gradient from 5-30% buffer B in 95min
1034 followed by an increase to 60% for 5min, and by a 5min wash at 95% buffer B at 300nl/min
1035 (Buffer A: 0.1% Formic Acid, 99.9% ddH₂O; Buffer B: 0.1% Formic Acid, 80% CAN, 19.9%
1036 ddH₂O). The column temperature was kept at 60°C by an in-house manufactured oven.

1037 Mass spectrometry analysis was performed in a data-dependent PASEF mode with 1 MS1
1038 survey TIMS-MS and 10 PASEF MS/MS scans per acquisition cycle. Ion accumulation and
1039 ramp time in the dual TIMS analyzer was set to 100ms each and we analyzed the ion mobility
1040 range from $1/K_0 = 1.6 \text{ Vs cm}^{-2}$ to 0.6 Vs cm^{-2} . Precursor ions for MS/MS analysis were isolated
1041 with 2Th windows for $m/z < 700$ and 3Th for $m/z > 700$ in a total m/z range of 100-1,700 by
1042 synchronizing quadrupole switching events with the precursor elution profile from the TIMS
1043 device. The collision energy was lowered linearly as a function of increasing mobility starting
1044 from 59 eV at $1/K_0 = 1.6 \text{ VS cm}^{-2}$ to 20 eV at $1/K_0 = 0.6 \text{ Vs cm}^{-2}$. Singly charged precursor ions
1045 were excluded with a polygon filter (otof control, Bruker Daltonik GmbH). Precursors for MS/MS
1046 were picked at an intensity threshold of 2.500 a.u. and resequenced until reaching a 'target
1047 value' of 20,000 a.u taking into account a dynamic exclusion of 40sec elution²⁵.

1048 Before MS analysis, the LC-MS setup was subjected to a rigorous quality control procedure.
1049 These criteria included protein- and peptide-identifications as well as general technical
1050 specifications like chromatography performance. If those thresholds were met (>5.500 protein
1051 groups, >38.000 peptides from 200 ng tryptic HeLa digest, chromatographic peak FWHM of ≤ 9
1052 sec and peak base-to-base width ≤ 17 sec on a 120 min liquid chromatography gradient;
1053 Quantitative reproducibility across two subsequent QC runs with a Pearson correlation of > 0.97
1054 and coefficients of variation of $\leq 10\%$) the project measurements were initiated. Furthermore,

1055 we subject our instruments to a rigorous weekly maintenance procedure (Maintenance of the
1056 Liquid chromatography platform and re-calibration of the mass spectrometer) to ensure highest
1057 overall performance and reproducibility.

1058 Proteomics raw file processing

1059 Raw files were searched against the human Uniprot databases (UP000005640_9606.fa,
1060 UP000005640_9606_additional.fa) MaxQuant (Version 1.6.7), which extracts features from
1061 four-dimensional isotope patterns and associated MS/MS spectra⁵⁹. False-discovery rates were
1062 controlled at 1% both on peptide spectral match (PSM) and protein level. Peptides with a
1063 minimum length of seven amino acids were considered for the search including N-terminal
1064 acetylation and methionine oxidation as variable modifications and cysteine
1065 carbamidomethylation as fixed modification, while limiting the maximum peptide mass to 4,600
1066 Da. Enzyme specificity was set to trypsin cleaving c-terminal to arginine and lysine. A maximum
1067 of two missed cleavages were allowed. Maximum precursor and fragment ion mass tolerance
1068 were searched as default for TIMS-DDA data, while the main search peptide tolerance was set
1069 to 20ppm. The median absolute mass deviation for the data was 0.68ppm. Peptide
1070 identifications by MS/MS were transferred by matching four-dimensional isotope patterns
1071 between the runs with a 0.7-min retention-time match window and a 0.05 1/K₀ ion mobility
1072 window⁶⁰. Label-free quantification was performed with the MaxLFQ algorithm and a minimum
1073 ratio count of 1⁶¹.

1074 Bioinformatic analysis

1075 Bioinformatics analysis was performed in Perseus (version 1.6.7.0 and 1.5.5.0) and GraphPad
1076 Prism (version 8.2.1)⁶². Reverse database, contaminant, and only by site modification
1077 identifications were removed from the dataset. Data were grouped by analytical replicates and
1078 filtered to at least 70% data completeness in one group. Missing values were imputed from a

1079 data table specific normal distribution estimate with a downshift of 1.8 and a width of 0.3
1080 standard deviations after \log_2 -transformation of the data. To represent the data reproducibility
1081 and variability, a principal component analysis was performed on the median data of analytical
1082 replicate measurements of each individual. Clinically classified T2D and ND individuals were
1083 tested for differences in their mean by a two-sided Student's t-test with $S_0=0.1$ and a Benjamini-
1084 Hochberg correction for multiple hypothesis testing at an FDR of 0.05 preserving grouping of
1085 each individuals analytical replicate measurements, and presented as volcano plot. We then
1086 normalized the data by row-wise z-scoring followed by hierarchical clustering using Euclidean
1087 as the distance parameter for column- and row-wise clustering. 1D gene ontology enrichments
1088 of clustered and systematically changed proteins were performed with regards to their cellular
1089 compartment and keywords assignment³⁰. \log_2 transformed LFQ data were used for the
1090 calculation of intensity shifts of the enriched keyword or cellular compartment term for each of
1091 the displayed clusters. Total protein copy number estimation of the median LFQ intensities for
1092 patients clinically classified as non-diabetic and diabetic were calculated using the Perseus
1093 plugin 'Proteomic ruler'²⁹. Median LFQ intensity values for all T2D and ND were calculated. We
1094 annotated protein groups for the leading protein ID with the human Uniprot fasta file
1095 (UP000005640_9606.fa) and estimated the protein copy number with the following settings:
1096 Averaging mode. 'All columns separately', Molecular masses: 'Average molecular mass',
1097 Detectability correction: 'Number of theoretical peptides', Scaling mode: 'Histone proteomic
1098 ruler', Ploidy: '2', Total cellular protein concentration: '200g/l'. Proteins were annotated with
1099 regards to their cellular compartment by gene ontology. We calculated the median protein copy
1100 number for the samples from T2D and ND PPP separately and multiplied it by its protein mass.
1101 To calculate the subcellular protein mass contribution, we calculated the protein mass
1102 proportion for the GOCC terms 'Nucleus', 'Mitochondrion', 'Cytoskeleton', 'Golgi apparatus', and
1103 'Endoplasmic reticulum'. For calculating the organellar change between T2D and ND PPP,
1104 protein mass contributions of each organelle were normalized by its respective 'Nuclear part'

1105 contribution. Chromosomal annotation of significantly changed proteins between T2D and ND
1106 PPP was identified via Ensembl ID. For transcriptome to proteome correlation, the gene
1107 intersection of both data sets was scaled to 1E6 units, followed by log₁₀-transformation.

1108 Antibody validation

1109 Rabbit polyclonal anti-ALDOB antibody (Proteintech, Cat.No. 18065-1-AP) was tested for
1110 specificity by western blotting of protein extracts of *ALDOB*^{-/-} MIN6 cells generated with a
1111 CRISPR/Cas9 system, as described⁶³. Primary antibodies against ALDOB, ALDOA (Abnova,
1112 Cat. No. H00000226-M01) and gamma tubulin as loading control (Sigma Aldrich, Cat.No. T-
1113 6557) were diluted in 5% non-fat milk 1:2000, 1:1000 and 1:5000, respectively. The knock-out of
1114 *ALDOB* was verified by Sanger sequencing of the target locus.

1115 Isolated mouse islet and cell line experiments

1116 Mouse (C57BL/6J, db/db (BKS.Cg-Dock7^m +/+ Lepr^{db}/J) and db/+ (Charles River Laboratories),
1117 3 animals/strain, male, age 13 weeks) islets were cultured for 1 day post isolation. Islet beta
1118 MIN6c4 (MIN6 clone 4, from Osaka University under Material License Agreement) and alpha
1119 αTC1-clone 6 (ATCC, CRL-2934) cell lines were harvested for RNA extraction using Qiagen
1120 RNeasy Mini Kit according to the manufacturer's instructions. After quality control, RNA samples
1121 were sequenced using the Illumina HiSeq 2000 platform and processed as previously
1122 described^{51,64,65}. All animal experiments were done in accordance with the ethical approval of
1123 the Sanofi-Aventis Animal Welfare Office, Frankfurt/Main, Germany. The animals were housed
1124 at 20-24°C, by 45-65 % humidity setting in an artificial day / night (12hrs) rhythm.

1125 Immunofluorescence microscopy

1126 Immunofluorescence staining was done on formalin-fixed paraffin embedded 5µm thick sections
1127 of human pancreatic tissue. Acetylated histone H3 and H4 were detected in separate sections

1128 using rabbit polyclonal antibodies (Merck Millipore Cat.No. 06-598 and 06-599, respectively,
1129 dilution 1:100). A mouse monoclonal anti-insulin antibody (Thermo Fisher Scientific Cat.No. 53-
1130 9769-82, dilution 1:200) was used for co-staining, to identify the beta cell areas. Images were
1131 acquired using a Nikon C2+ confocal microscope with a 60x oil immersion objective, with
1132 acquisition parameters normalized to a negative control sample.

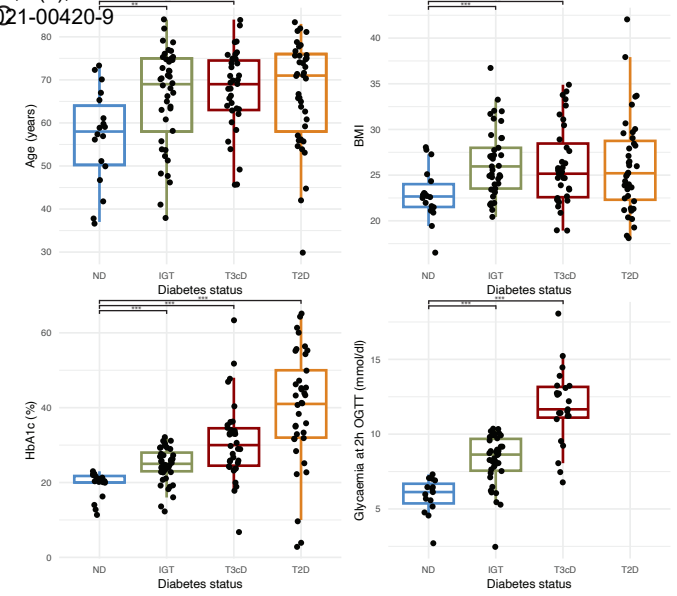
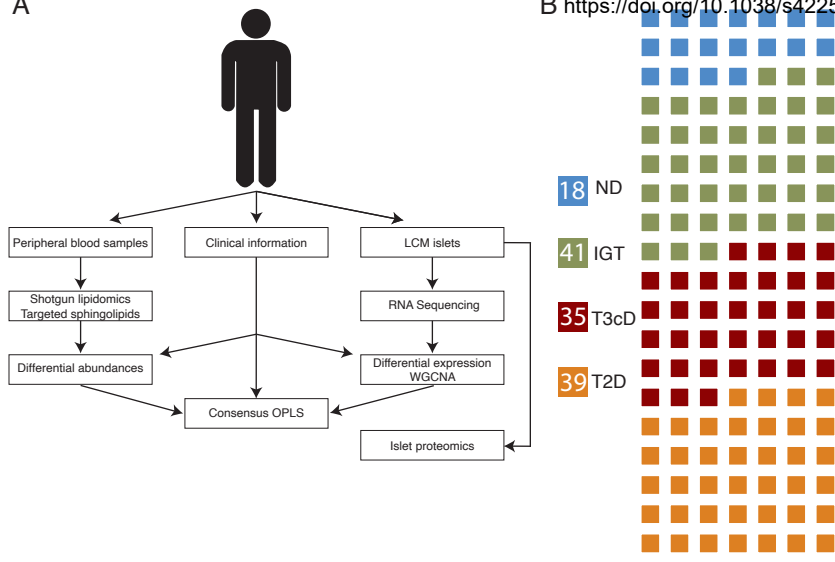
1133 Materials and methods references

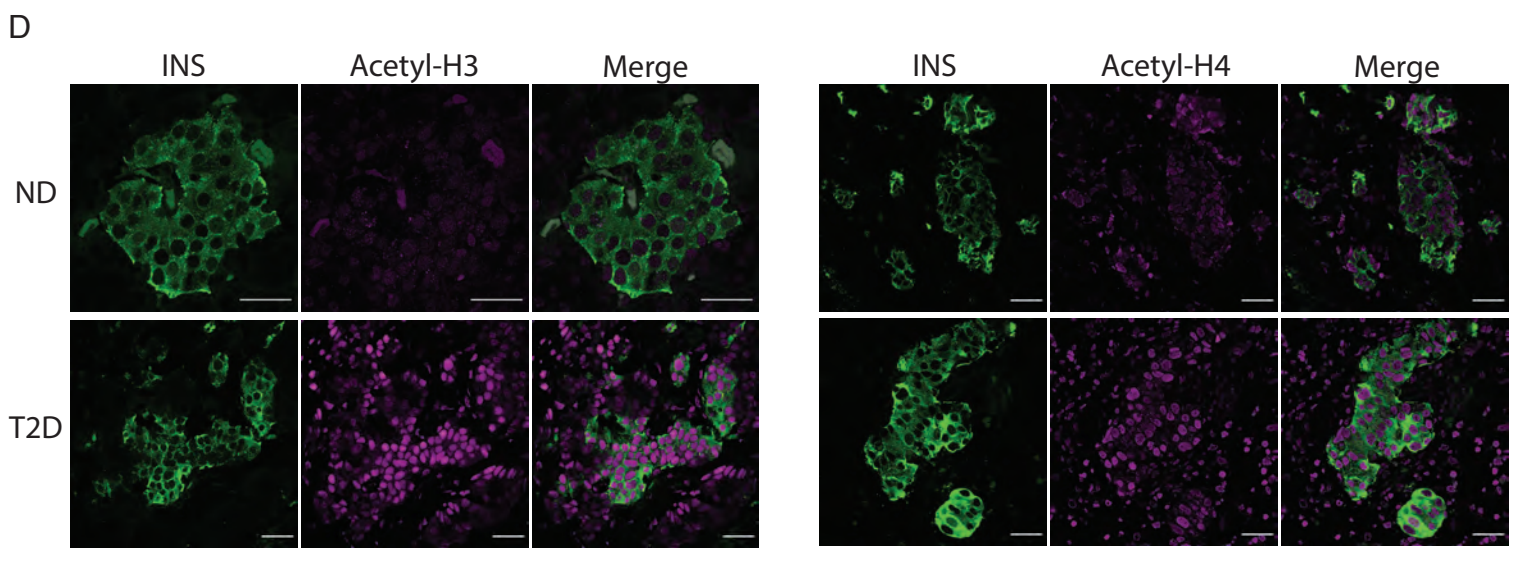
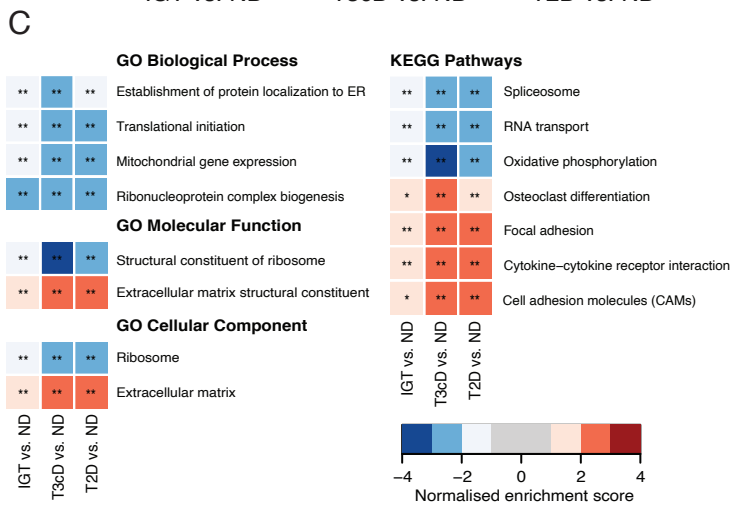
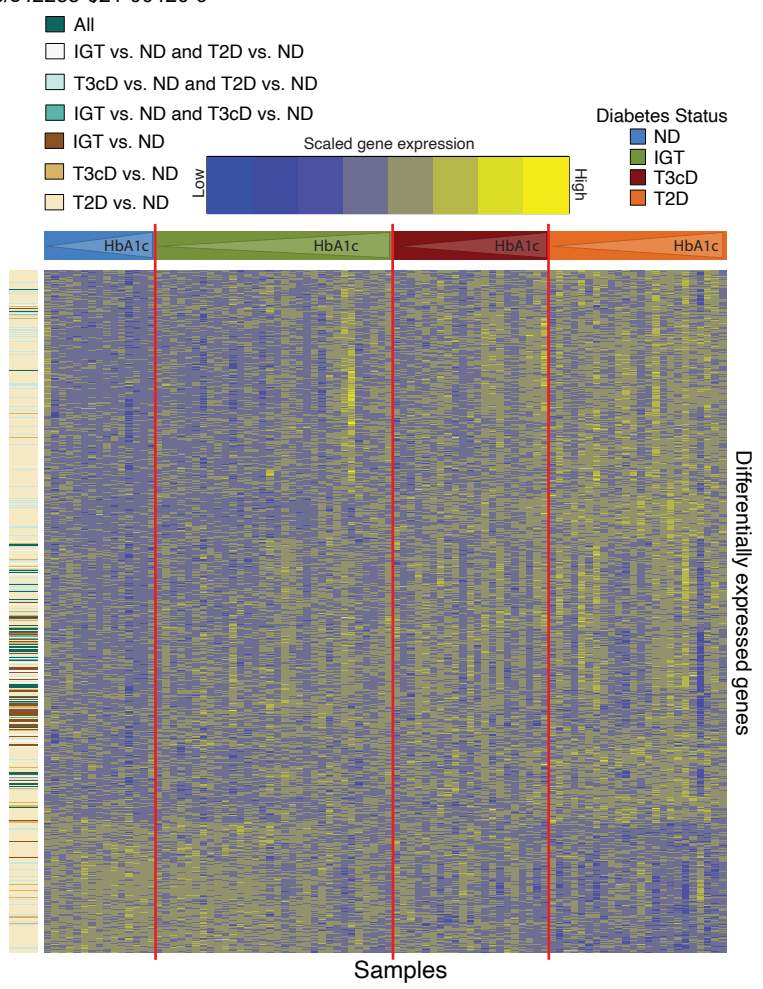
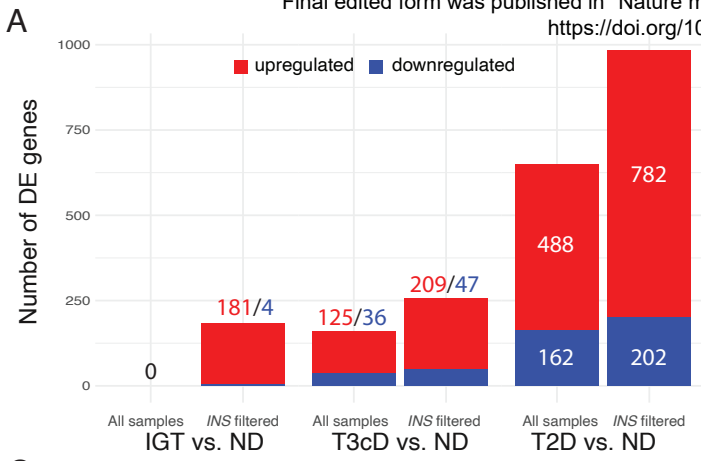
- 1134 44. Sturm, D. *et al.* Improved Protocol For Laser Microdissection Of Human Pancreatic Islets
1135 From Surgical Specimens. *J. Vis. Exp.* 2–7 (2013). doi:10.3791/50231
- 1136 45. Martin, M. Cutadapt removes adapter sequences from high-throughput sequencing
1137 reads. *EMBnet.journal; Vol 17, No 1 Next Gener. Seq. Data Anal.* - 10.14806/ej.17.1.200
1138 (2011).
- 1139 46. Wingett, S. W. & Andrews, S. FastQ Screen: A tool for multi-genome mapping and quality
1140 control. *F1000Research* 7, 1338 (2018).
- 1141 47. Davis, M. P. A., van Dongen, S., Abreu-Goodger, C., Bartonicek, N. & Enright, A. J.
1142 Kraken: A set of tools for quality control and analysis of high-throughput sequence data.
1143 *Methods* 63, 41–49 (2013).
- 1144 48. Dobin, A. *et al.* STAR: Ultrafast universal RNA-seq aligner. *Bioinformatics* 29, 15–21
1145 (2013).
- 1146 49. Anders, S., Pyl, P. T. & Huber, W. HTSeq-A Python framework to work with high-
1147 throughput sequencing data. *Bioinformatics* 31, 166–169 (2015).
- 1148 50. Wang, L., Wang, S. & Li, W. RSeQC: Quality control of RNA-seq experiments.
1149 *Bioinformatics* 28, 2184–2185 (2012).
- 1150 51. Love, M. I., Huber, W. & Anders, S. Moderated estimation of fold change and dispersion
1151 for RNA-seq data with DESeq2. *Genome Biol.* 15, (2014).
- 1152 52. Ritchie, M. E. *et al.* Limma powers differential expression analyses for RNA-sequencing

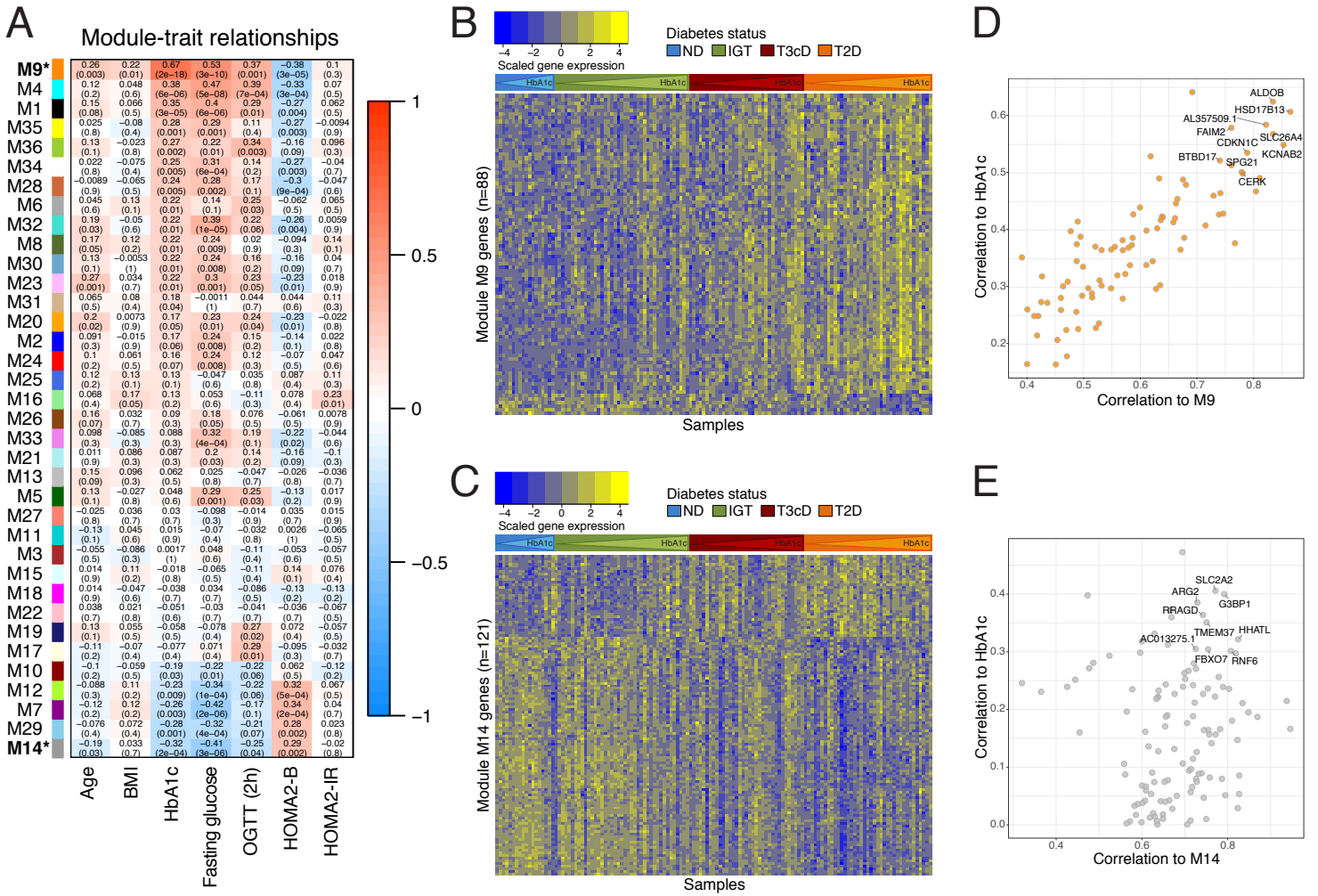
- 1153 and microarray studies. *Nucleic Acids Res.* **43**, e47 (2015).
- 1154 53. Smyth, G. K. *et al.* RNA-seq analysis is easy as 1-2-3 with limma, Glimma and edgeR.
1155 *F1000Research* **5**, (2018).
- 1156 54. Yu, G., Wang, L. G., Han, Y. & He, Q. Y. ClusterProfiler: An R package for comparing
1157 biological themes among gene clusters. *Omi. A J. Integr. Biol.* **16**, 284–287 (2012).
- 1158 55. Surma, M. A. *et al.* An automated shotgun lipidomics platform for high throughput,
1159 comprehensive, and quantitative analysis of blood plasma intact lipids. *Eur. J. Lipid Sci.*
1160 *Technol.* **117**, 1540–1549 (2015).
- 1161 56. Smilde, A. K., Kiers, H. A. L., Bijlsma, S., Rubingh, C. M. & Van Erk, M. J. Matrix
1162 correlations for high-dimensional data: The modified RV-coefficient. *Bioinformatics* **25**,
1163 401–405 (2009).
- 1164 57. Bylesjö, M., Rantalainen, M., Nicholson, J. K., Holmes, E. & Trygg, J. K-OPLS package:
1165 Kernel-based orthogonal projections to latent structures for prediction and interpretation
1166 in feature space. *BMC Bioinformatics* **9**, (2008).
- 1167 58. Kulak, N. A., Pichler, G., Paron, I., Nagaraj, N. & Mann, M. Minimal, encapsulated
1168 proteomic-sample processing applied to copy-number estimation in eukaryotic cells. *Nat.*
1169 *Methods* **11**, 319–324 (2014).
- 1170 59. Cox, J. & Mann, M. MaxQuant enables high peptide identification rates, individualized
1171 p.p.b.-range mass accuracies and proteome-wide protein quantification. *Nat. Biotechnol.*
1172 **26**, 1367–1372 (2008).
- 1173 60. Prianichnikov, N. *et al.* Maxquant software for ion mobility enhanced shotgun proteomics.
1174 *Mol. Cell. Proteomics* **19**, 1058–1069 (2020).
- 1175 61. Cox, J. *et al.* Accurate proteome-wide label-free quantification by delayed normalization
1176 and maximal peptide ratio extraction, termed MaxLFQ. *Mol. Cell. Proteomics* **13**, 2513–
1177 2526 (2014).
- 1178 62. Tyanova, S. *et al.* The Perseus computational platform for comprehensive analysis of

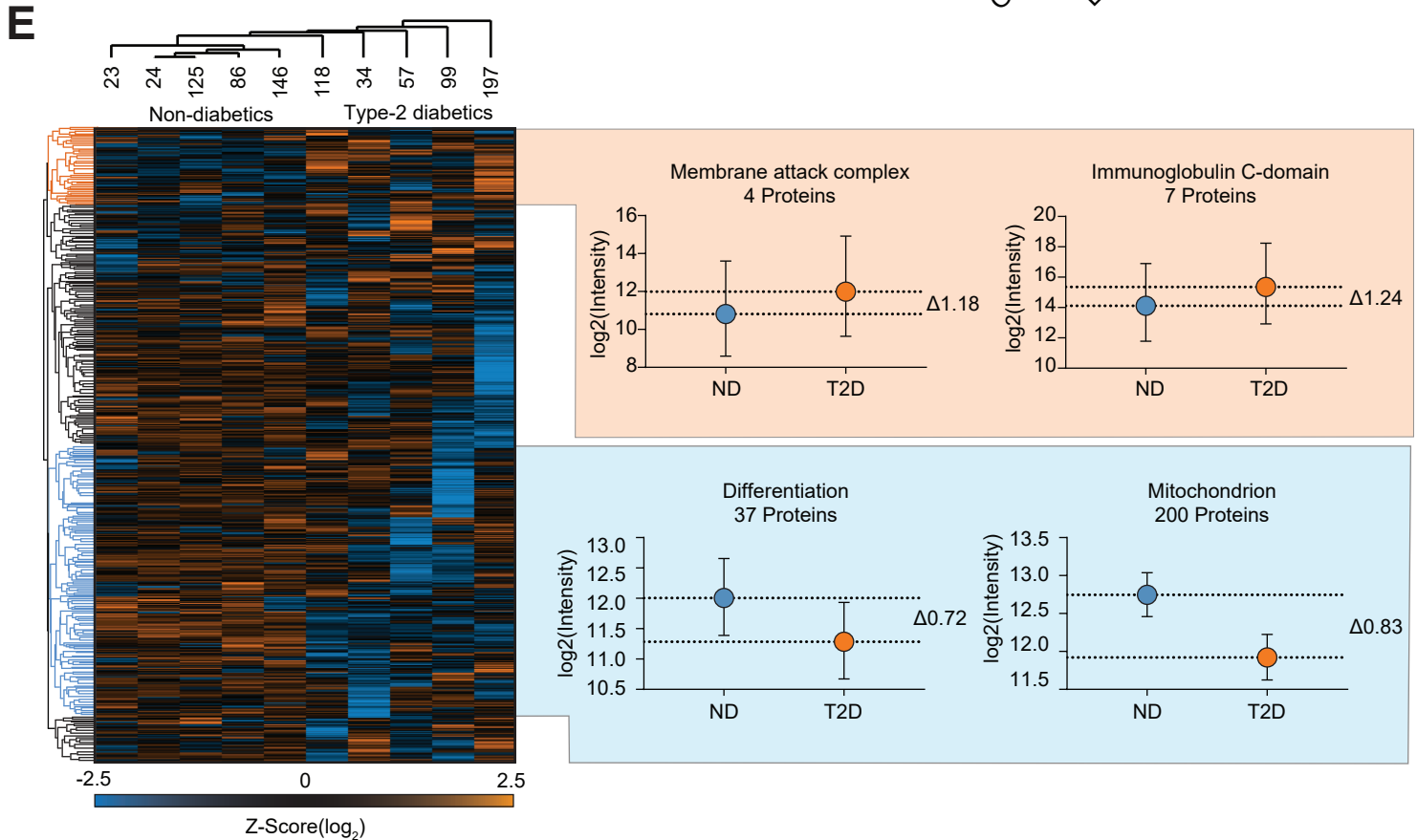
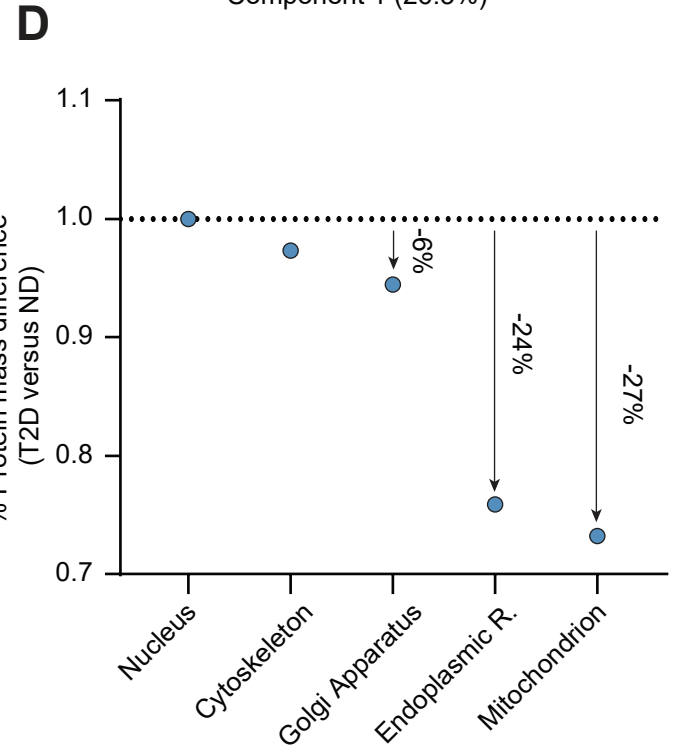
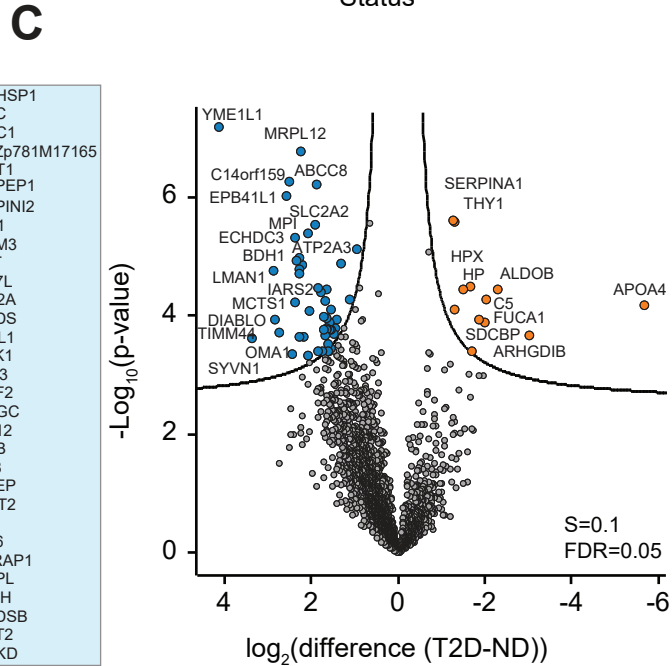
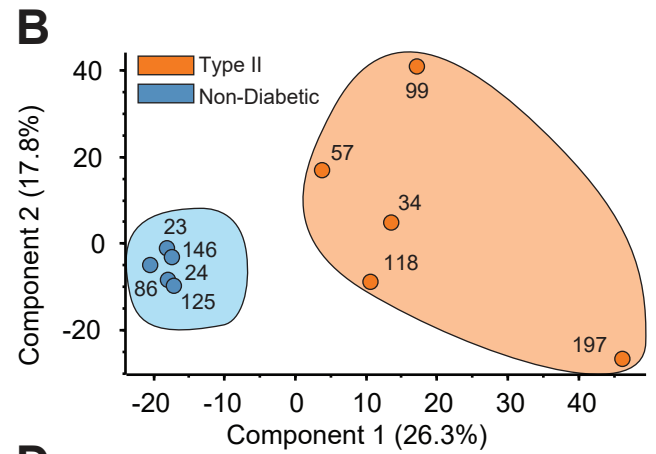
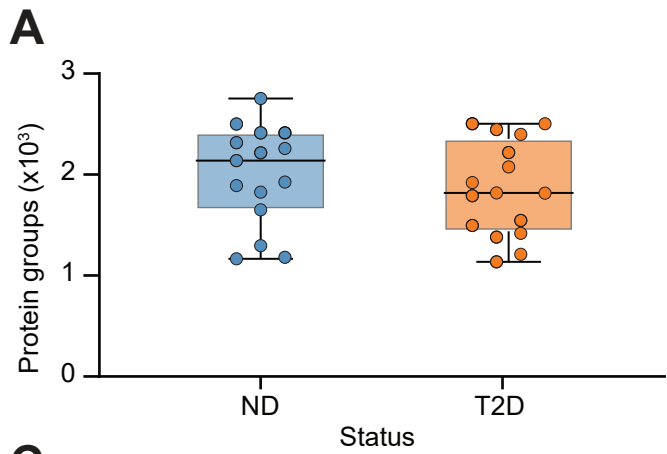
- 1179 (prote)omics data. *Nature Methods* **13**, 731–740 (2016).
- 1180 63. Ran, F. A. *et al.* Genome engineering using the CRISPR-Cas9 system. *Nat. Protoc.* **8**,
1181 2281–2308 (2013).
- 1182 64. Hu, J., Ge, H., Newman, M. & Liu, K. OSA: A fast and accurate alignment tool for RNA-
1183 Seq. *Bioinformatics* **28**, 1933–1934 (2012).
- 1184 65. Li, B., Ruotti, V., Stewart, R. M., Thomson, J. A. & Dewey, C. N. RNA-Seq gene
1185 expression estimation with read mapping uncertainty. *Bioinformatics* **26**, 493–500 (2009).
1186

A

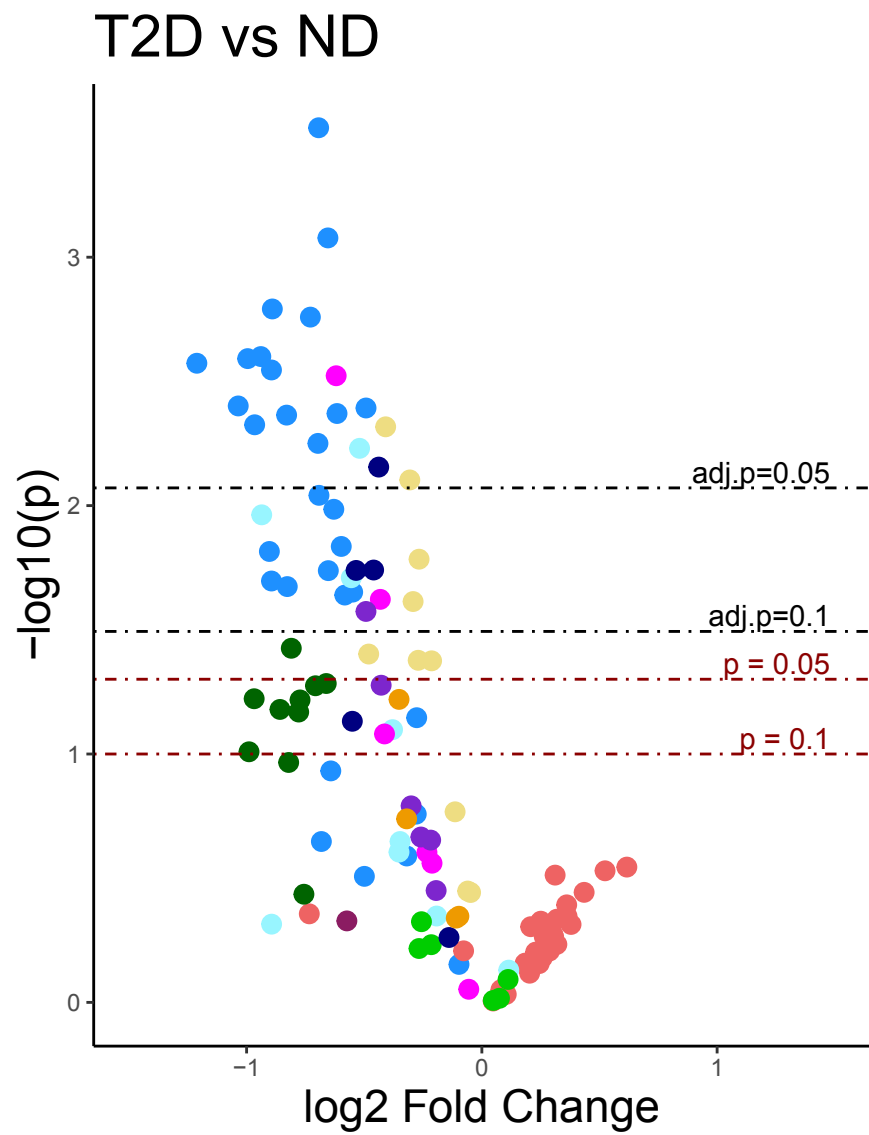




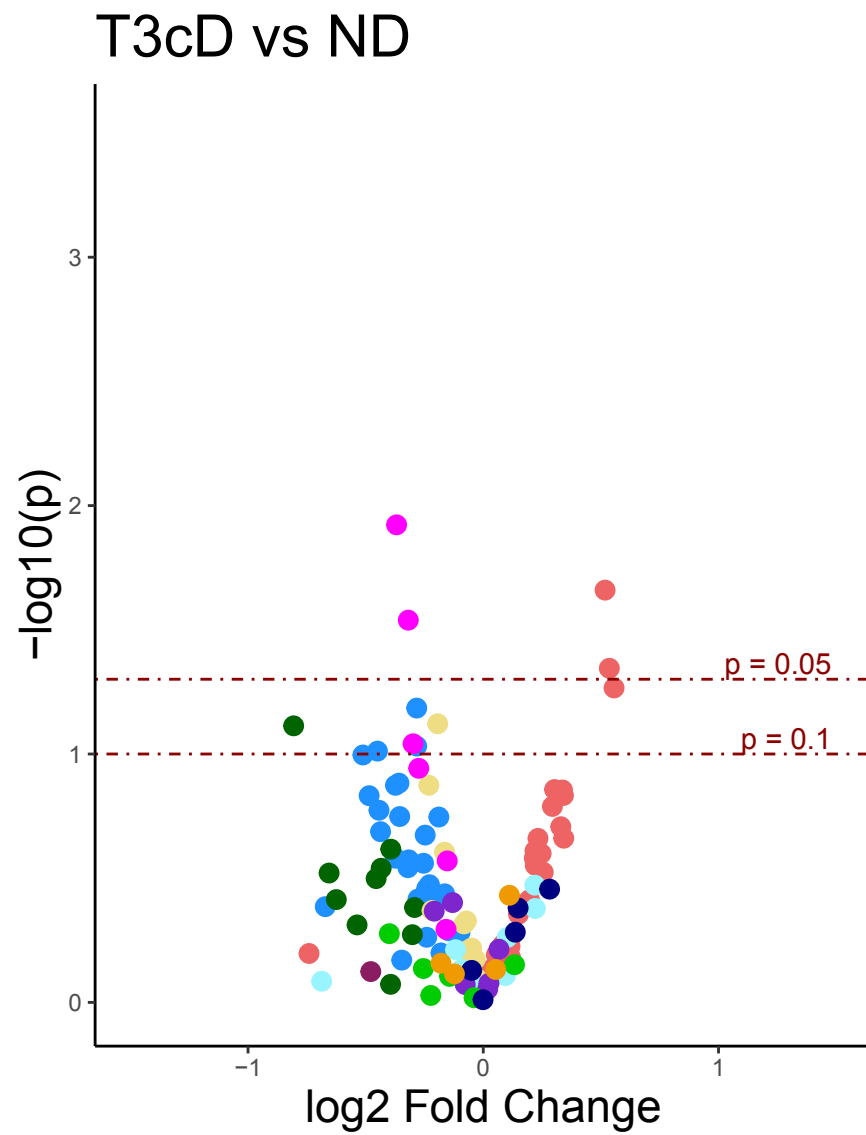




A)



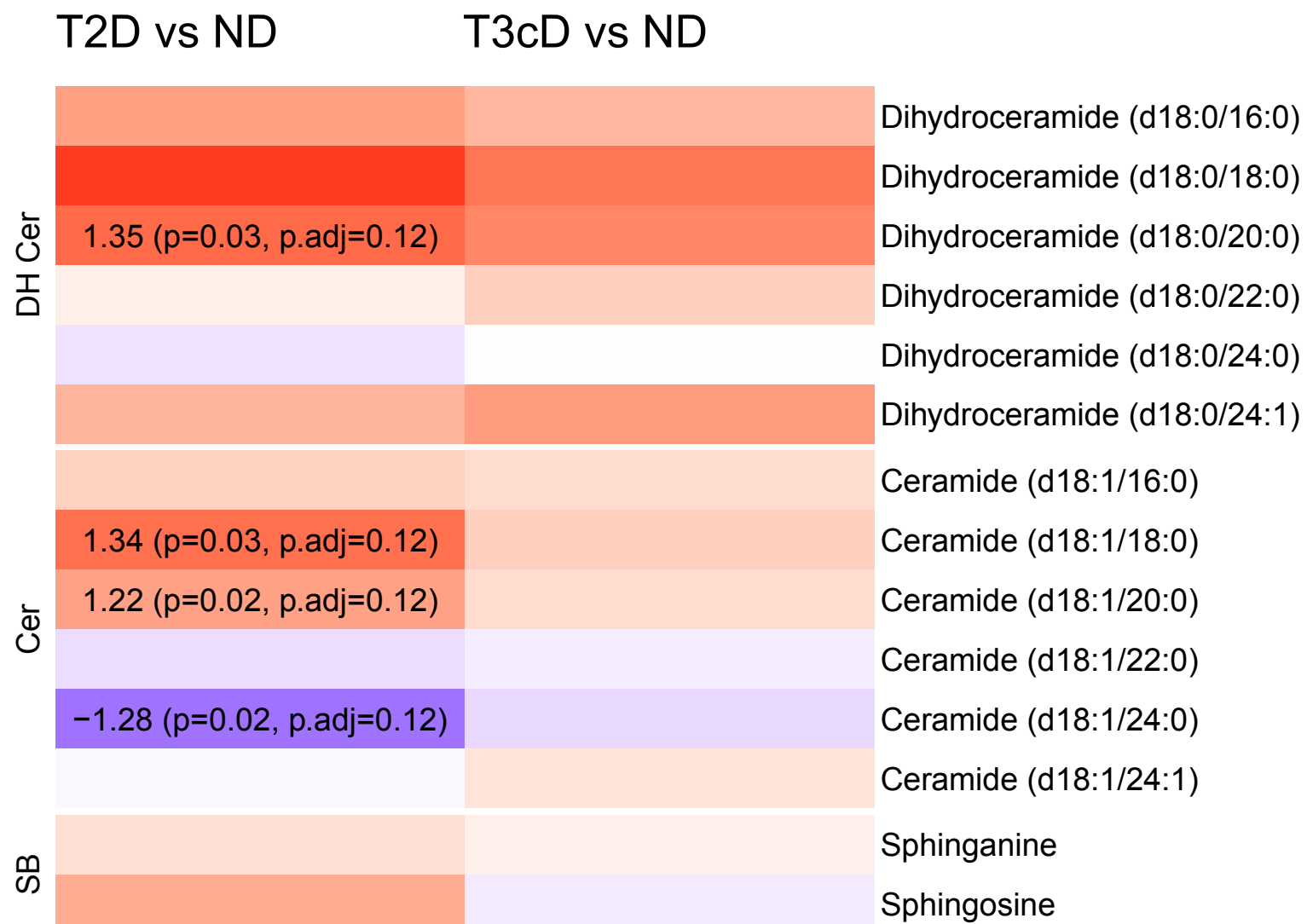
B)



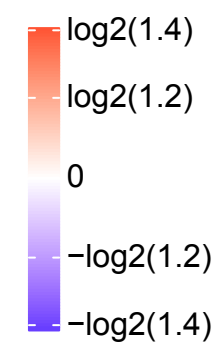
Shotgun Lipidomics Color Codes

- Cer
- DAG
- LPC
- LPE
- PC
- PC O-
- PE
- PE O-
- PI
- SM
- TAG

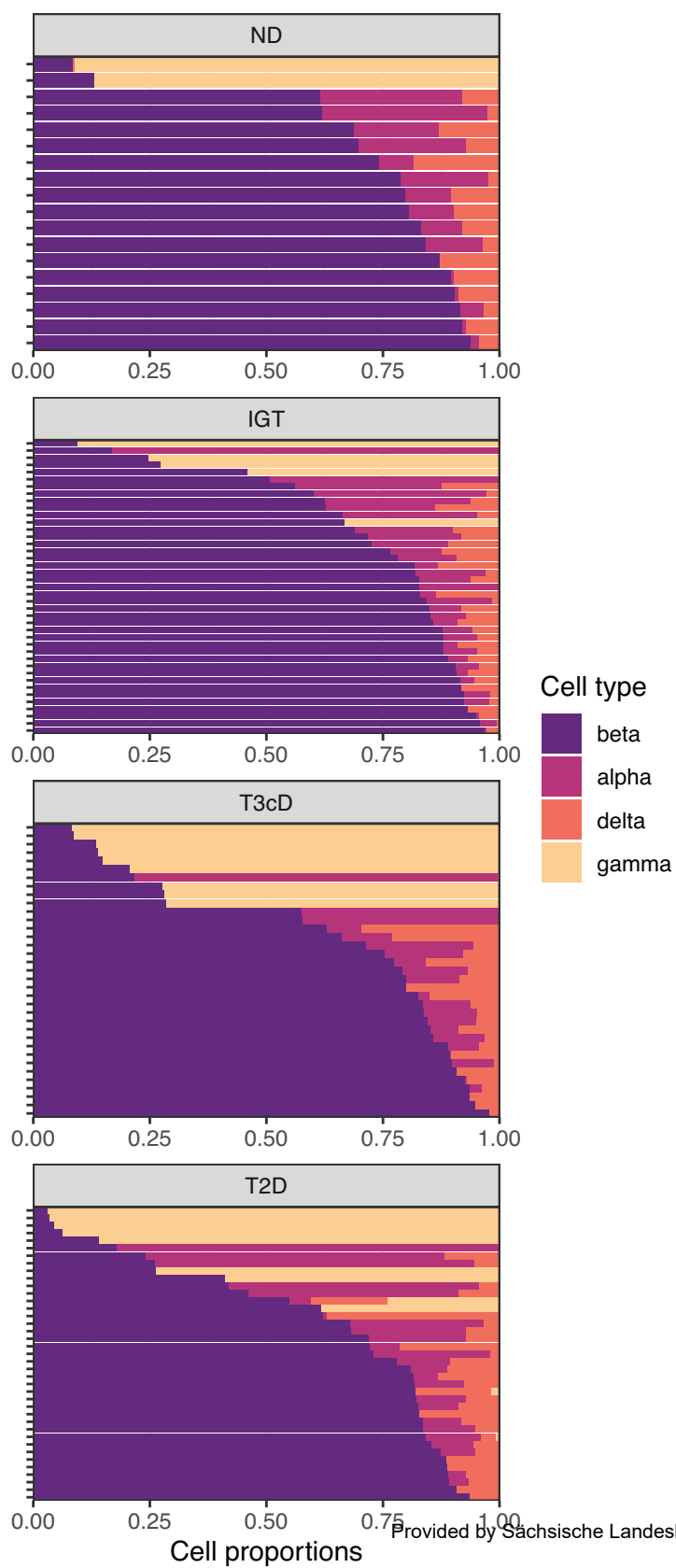
C)



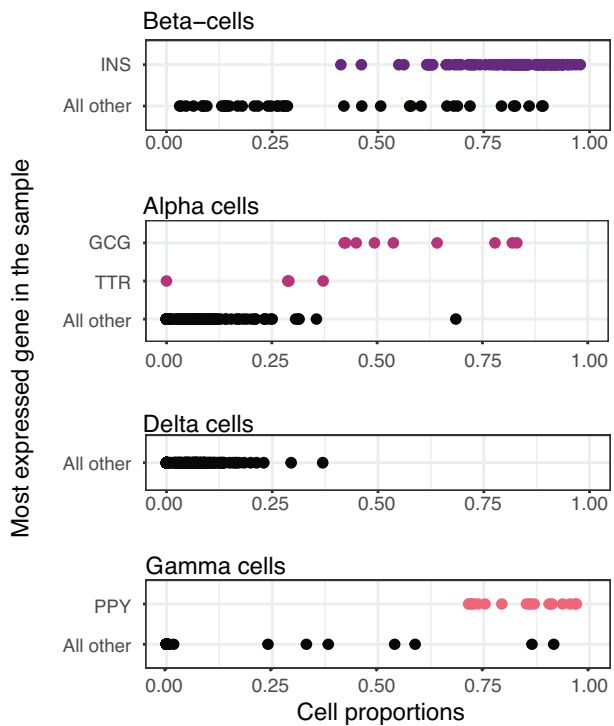
Targeted Sphingolipid Analysis Log₂ Fold Change



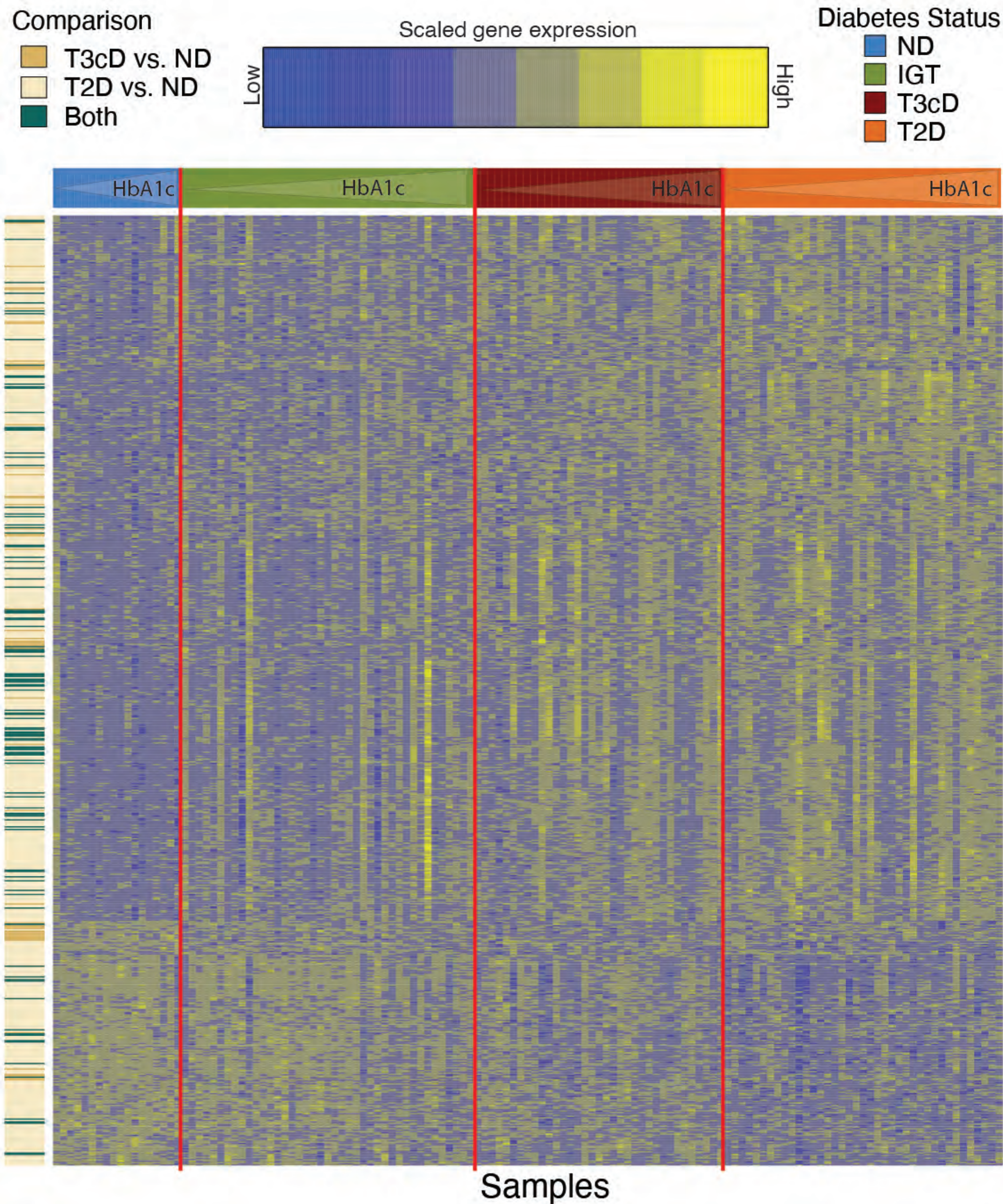
A



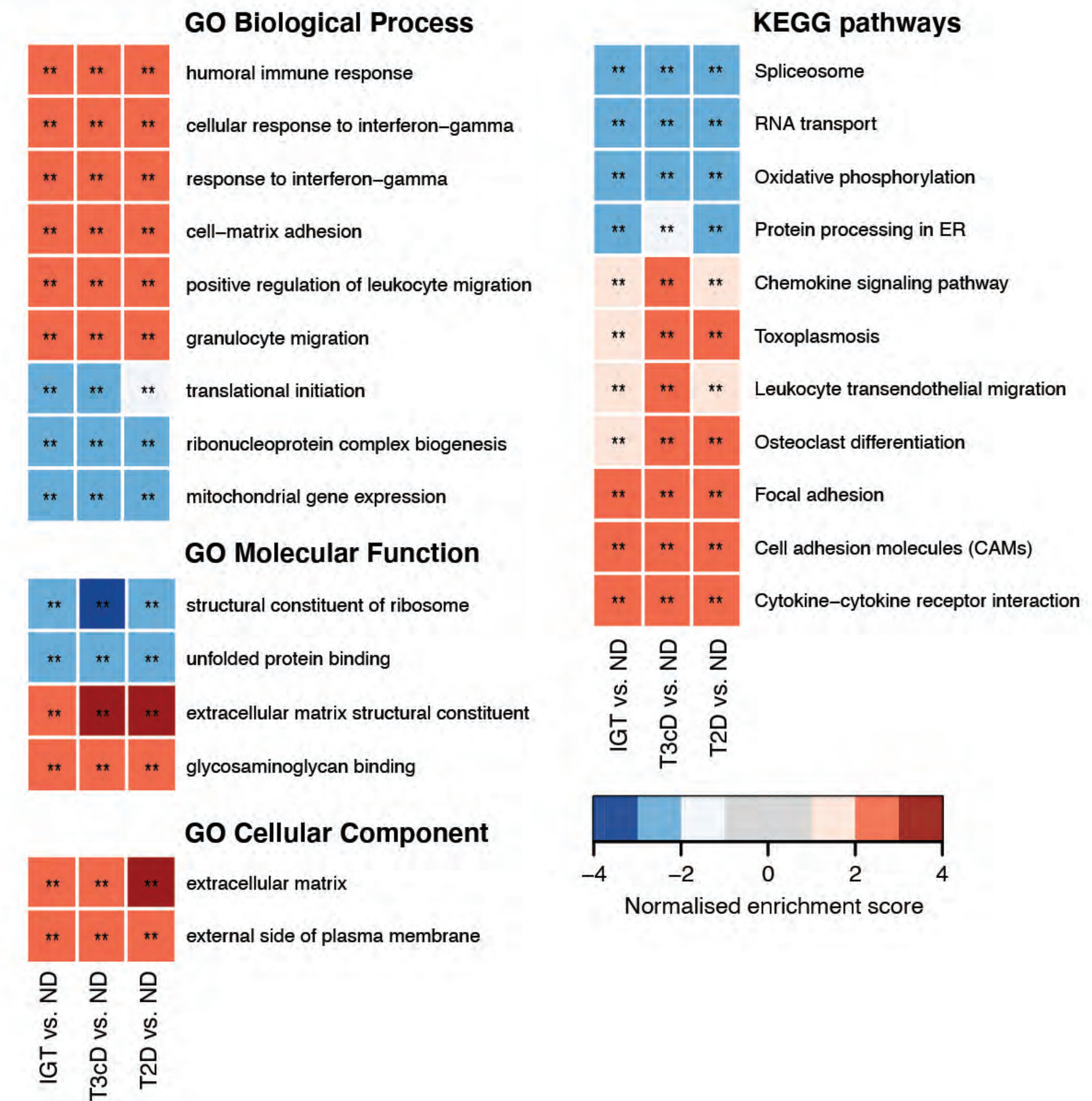
B



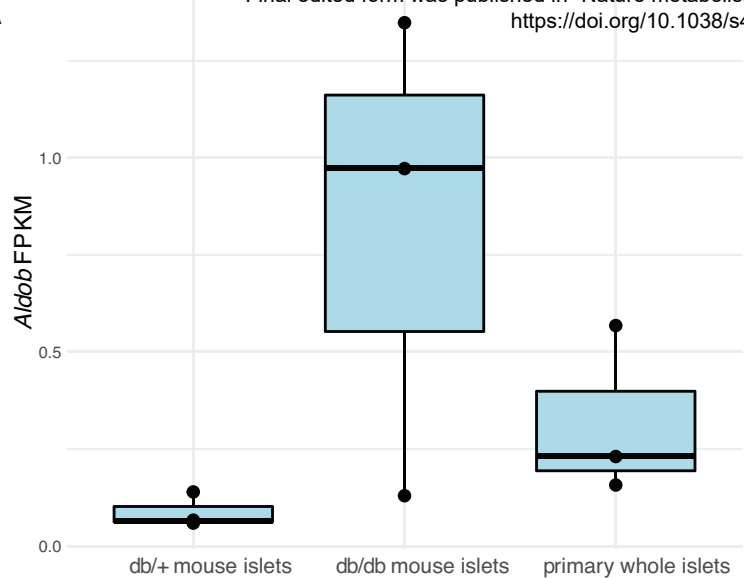
A



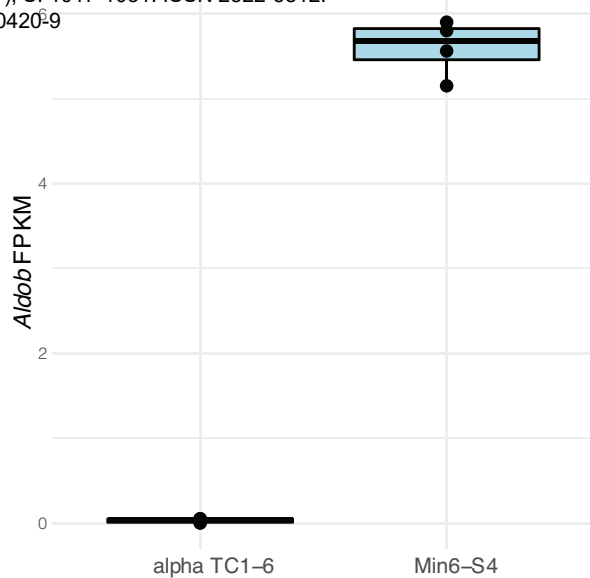
B



A



B



C

